MERCATOR
Quarterly Newsletter

Editorial – January 2009

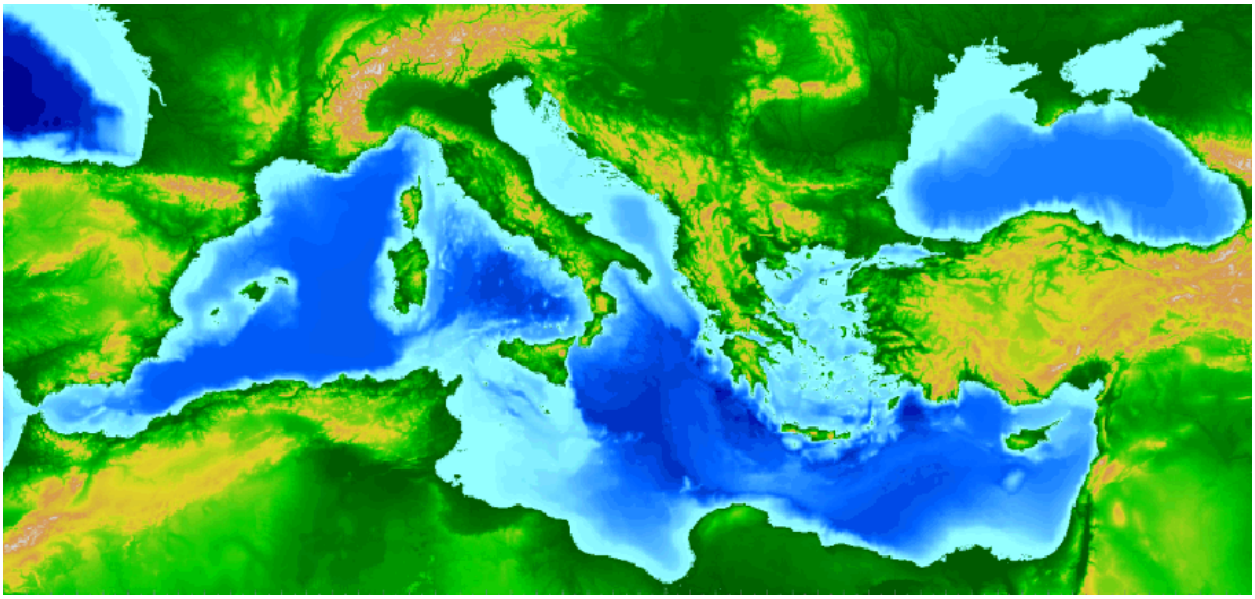

Credits: CIESM/Ifremer

Greetings all,

This month's newsletter is devoted to the Mediterranean Sea and its various faces.

As an introduction, an article by Drobinski et al. presents the HYMEX program (HYdrological cycle in Mediterranean Experiment) which is aiming at better understanding the global water cycle in the Mediterranean region. The next article by Langlais et al. is dealing with a high resolution coastal and shelf model in the Gulf of Lions. Then, Boy et al. are describing the input from spatial gravimetry to better represent the ocean circulation in the Mediterranean Sea. The next article by D'Ovidio et al. is telling us about tracer frontal structures induced by altimeter velocities with a lagrangian technique in the Eastern Mediterranean Sea. The last article by L'Hévéder et al. is dealing with operational forecast of glider trajectories in the Mediterranean Sea using the Mercator forecasts.

The next April 2009 newsletter will review the current work on ocean indices aiming at better understanding the state of the ocean climate.

We wish you a pleasant reading.

Contents

The HyMeX (Hydrological Cycle in the Mediterranean Experiment) program: The specific context of oceanography 3

By Philippe Drobinski et al

Towards high resolution coastal and shelf circulation modeling: impact of the atmospheric forcing resolution in the Gulf of Lions 5

By Clothilde Langlais, Bernard Barnier and Philippe Fraunie

Ocean circulation in the Mediterranean Sea: Input from Spatial Gravimetry 14

By Jean-Paul Boy, David Garcia, Scott B.Luthcke, David D. Rowlands and Douglas S. Chinn

Lagrangian Validation of the Mediterranean Mean Dynamic Topography by extraction of Tracer Frontal Structures..... 24

By Francesco d'Ovidio, Vincent Taillandier, Isabelle Taupier-Letage and Laurent Mortier

Operational Forecast of Glider trajectories during EGO 2008 operations in the Mediterranean Sea using Mercator Ocean Forecast 33

By Blandine l'Hévéder, Jean-Michel Lellouche, Pascale Lherminier, Laurent Mortier, Thierry Terre, Pierre Testor and Gaëtan Vinay

Notebook 39

The HyMeX (Hydrological Cycle in the Mediterranean Experiment) program: The specific context of oceanography

By Philippe Drobinski[1], Karine Béranger[2,3], Véronique Ducrocq[4], John T. Allen[5], Georges Chronis[6], Jordi Font[7], Gurvan Madec[3], Evangelos Papathanassiou[6], Nadia Pinardi[8], Cherif Sammari[9], Isabelle Taupier-Letage[10]

[1]. Laboratoire de Météorologie Dynamique/Institut Pierre Simon Laplace, Ecole Polytechnique, Palaiseau, France
[2]. Unité de Mécanique, Ecole Nationale Supérieure de Techniques Avancées, Palaiseau, France
[3]. Laboratoire d'Océanographie et du Climat: Expérimentation et Approches Numériques/Institut Pierre Simon Laplace, Université Pierre et Marie Curie, Paris, France
[4]. Centre National de Recherches Météorologiques, Météo-France, 42 avenue Gustave Coriolis, 31057 Toulouse, France
[5]. National Oceanography Centre, Empress Dock – European way, SO143ZH Southampton, U.K.
[6]. Hellenic Centre for Marine Research, Greece
[7]. Institut de Ciencies del Mar, Dept. Physical Oceanography, Paseig maritim de la Barceloneta 37-49, 08003 Barcelona, Spain
[8]. Istituto Nazionale di Geofisica e Vulcanologia, Bologna, Italy
[9]. Institut National des Sciences et Technologies de la Mer, Tunis, Tunisia
[10]. Laboratoire d'Oceanographie et de Biogeochimie, Centre d'Oceanologie de Marseille, La Seyne sur Mer, France

In our climate change context, the hydrological cycle in the Mediterranean region is a key scientific, environmental and socio-economic question for a wide region including southern Europe, northern Africa and the Middle East. The Mediterranean region features a nearly closed sea surrounded by urbanized littorals and mountains from which numerous rivers originate. This results in a lot of interactions and feedbacks between oceanic, atmospheric, and hydrological processes which are perturbed by anthropogenic activities and play a predominant role on the regional climate and ecosystems. The Mediterranean climate is also influenced by both sub-tropical and mid-latitude climate dynamics and is therefore very sensitive to global climate change. The Mediterranean regions are also frequently affected by extreme weather events (heavy precipitation and flash-flooding, strong winds and large swell, droughts, etc) that regularly produce heavy damages and human losses. The ability to predict such dramatic events remains weak because of the contribution of very fine-scale processes and their non-linear interactions with the larger scale processes which are difficult and costly to resolve numerically.

The international scientific community has recognised the necessity to develop a major multi-disciplinary and multi-scale experimental project including enhanced and special observation periods with innovative instrumentation, to address the main issues related to the Mediterranean coupled system controlling the regional water cycle. The HyMeX project plans the monitoring of all relevant atmospheric, oceanic, hydrological and bio-chemical variables during a long observation period with additional and dedicated ground-based, shipborne and airborne means in 2011-2012 and 2012-2013. In this context, the HyMeX objectives are:

- to improve our understanding of the water cycle, with emphases on extreme events by monitoring and modeling the Mediterranean coupled system (atmosphere-land-ocean), its variability (from the event scale, to the seasonal and interannual scales) and characteristics over one decade in the context of global change,
- to evaluate the societal and economical vulnerability to extreme events and the adaptation capacity.

The multidisplinary research program and the database produced in the framework of HyMeX will facilitate the improvement of

- observational and modelling systems, especially of coupled systems. This requires new processes modelling, parameterization development, novel data assimilation systems for the different Earth compartments, reduction of uncertainty in climate modelling,
- the prediction capabilities of extreme events,
- the accurate simulation of the long-term water-cycle.

In the context of the HyMeX program, oceanographic research is thus a high priority. The Mediterranean sea is characterized by a negative water budget (evaporation excess over freshwater input by precipitation and runoff) balanced by a two-layer exchange at the Strait of Gibraltar composed of a warm and fresh upper water inflow from the Atlantic above a cooler and saltier Mediterranean outflow. Light and fresh Atlantic water is transformed into denser waters through interactions with the atmosphere that renew the Mediterranean waters at intermediate and deep levels, and generate the thermohaline circulation. Although the scheme of this thermohaline circulation is reasonably well drawn, little is known about its variability at seasonal and inter-annual scales and the role of the feedbacks between the Mediterranean Sea and the atmosphere on the water budget variability. The budget of the Mediterranean Sea has also to be examined in the context of the global warming, and in particular by highlighting the impact of an increase of the sea surface temperature on high-impact weather frequency and intensity. Indeed, the Mediterranean Sea is characterized by several key spots of intense sea-air exchanges associated with very strong

winds, which are caused by deep cyclogeneses or by the orographic response to the large scale forcing (Mistral, Bora, etc). These intense sea-air interactions and the associated sea surface cooling affect considerably the heat and water budgets of the Mediterranean Sea through the formation of dense or deep winter oceanic convection in coastal or offshore areas (Figure 1). Modifications of the oceanic mixed layer characteristics within the oceanic convection regions influence the lower part of the atmosphere. Hydrological and dynamical characteristics and inter-annual variability of the oceanic convection, as well as the strong wind systems, need to be better documented in order to stress the respective roles of the atmospheric forcing and oceanic processes, together with their interactions, and to progress in the modelling of these processes. These processes are modulated by the inputs of continental rivers and aquifers (biogeochemical and sediment transports), oceanic dynamics (boundary currents, submesocale, cascading) and feedbacks of aerosols and biomass. Ecosystems functioning are strongly related to this complex dynamic, which need to be better understood.

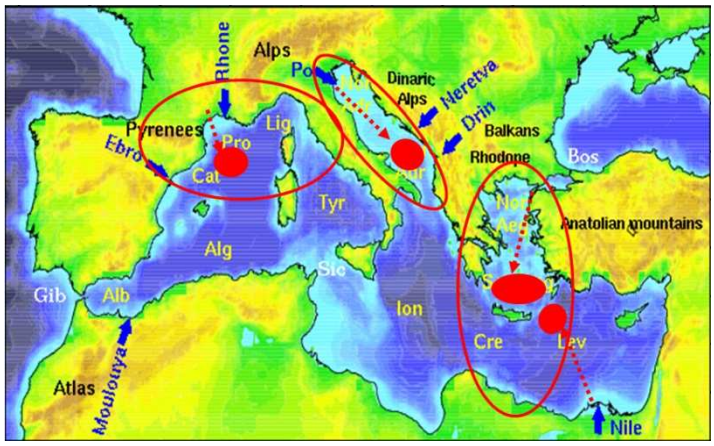

Figure 1

Zones of deep oceanic convection

In details, from an oceanographic perspective, the HyMeX program focuses on (1) the Mediterranean Sea response to strong wind forcing, (2) the air-sea feedbacks, (3) the modulation of the air-sea interactions by the runoff and ground water inputs to the sea, the slow branch of the Mediterranean water cycle, the ocean (sub)mesoscale dynamics, and the marine aerosols and ecosystems.

For this purpose, coupled simulations, properly configured and with relevant air-sea flux parameterizations, are needed to resolve the complex air-sea interactions, in particular to reproduce the interannual variability of thermohaline circulation and the observed trends in the Mediterranean water masses, and to be able to predict the evolution of the circulations in the context of climate change.

In this context, French scientists have decided to develop a new oceanic basin-scale Mediterranean model in collaboration with MERCATOR. This plateforme relying on the NEMO-MED12 model based on the NEMO (Nucleus for European Modeling of the Ocean) system at 1/12° (~ 7 km) horizontal resolut ion, will be dedicated to the forecasts of the basin-scale circulation, the basin-scale atmospheric forced/coupled oceanic circulation, the biogeochemical coupled oceanic circulation, the forcing of sub-basin scale oceanic models. These studies will be conducted in collaboration with Mediterranean partners in the framework of the HyMeX and MerMeX (Marine Ecosystems Response in the Mediterranean EXperiment) project preparations.

Towards high resolution coastal and shelf circulation modeling: impact of the atmospheric forcing resolution in the Gulf of Lions

By Clothilde Langlais[1,2,3], Bernard Barnier[1] and Philippe Fraunie[2]

[1] *LEGI, BP 53X, 1025 rue de la piscine, 38041 Grenoble Cedex 09, France*
[2] *LSEET, Universite du Sud Toulon Var, UMR CNRS 6017, BP 20132, 83957 La Garde Cedex, France*
[3] *actually at CSIRO, Castray Esplanad, GPO Box 1538, TAS 7000 Hobart, Australia*

Introduction

Questions of global changes entail elucidation of the mechanisms which control the exchanges at shelf breaks. Coastal areas and their inputs of freshwater, heat, biology and sediments are important boundary conditions for the open ocean. In the Gulf of Lions (in the North-western Mediterranean) (Red box on figure 1), a challenging topic is to improve the comprehension of the intermittent and fine scale processes acting on the continental shelf and their interactions with the along slope current (the North Mediterranean Current, NMC) and the bathymetry. A related scientific question is to evaluate the impact of those intermittent processes on the mean state and interannual variability of the circulation and hydrology.

With no significant tidal forcing, the ocean circulation on the shelf and at the shelf break is mainly driven by the atmospheric forcing with a large range of variability scales [Huthnance, 2002].

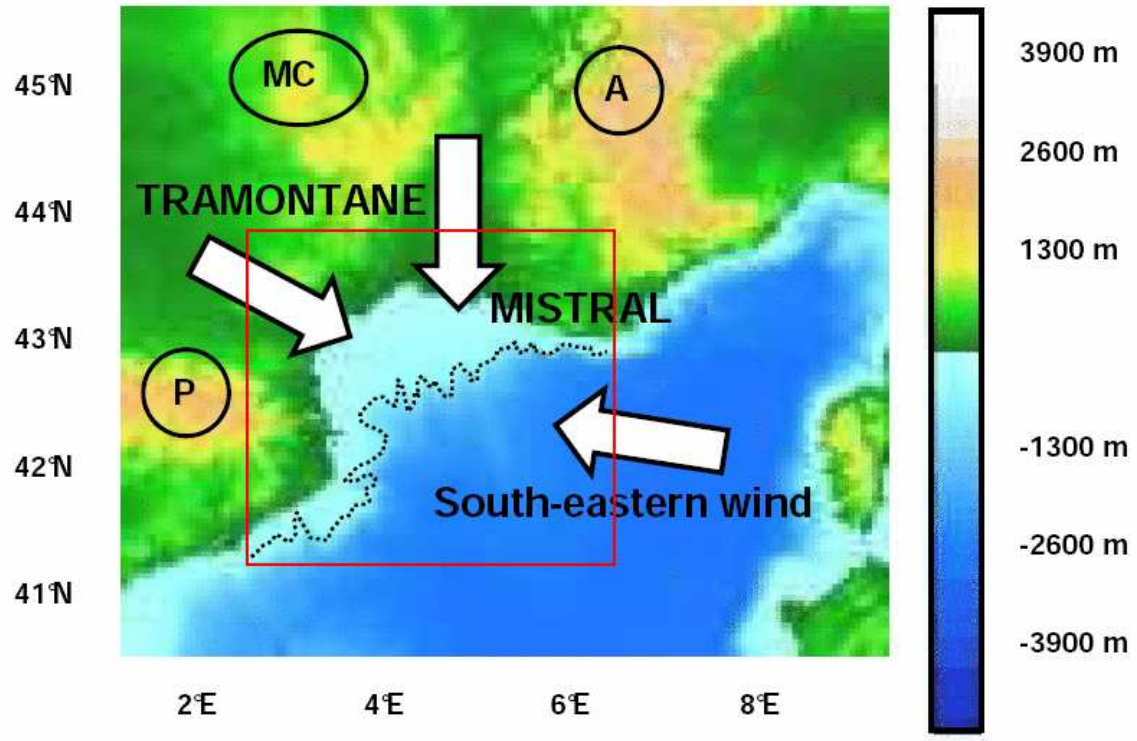

Figure 1

Schematic of the major winds acting in the Gulf of Lions: continental winds are channelled by the local orography and ocean winds mainly blowing from the south-east. The orography is characterized by the Alps (A), the Massif Central (MC) and the Pyrenees (P) mountains. The red box indicates the area referred to as the Gulf of Lions in this study. The dotted line crudely indicates the 250 m isobath, the boundary used to separate the shelf from the open ocean.

At the seasonal time scale, the full atmospheric forcing (heat, freshwater and wind) drives the variability of the coastal hydrology (involving the formation of a seasonal thermocline), the strength and variability of the NMC [Albérola et al., 1995 ; Flexas et al., 2002], the episodic formation of cold and dense water [Fieux, 1974 ; Mertens and Schott, 1998], and dense water cascading down the shelf break [Bethoux et al., 2002 ; Shapiro et al., 2003 ; Dufau-Julliand et al., 2004]. At time scales of few days, the wind is the main driving mechanism for the near coast up-and-downwelling systems [Millot, 1979; Johns et al., 1992], the positioning of Rhône river plume [Simpson, 1997; Reffray et al., 2004], the freshwater spreading and the exchanges across the shelf break. At even shorter time scales, solar radiation, thermal breezes and transient wind gusts generate strong inertial and

diurnal motions in the mixed layer [Millot and Crépon, 1981; VanHaren and Millot, 2003] with a noticeable impact on the sea surface temperature (SST).

Regarding the spatial patterns of the atmospheric forcing, the peculiar orography of surrounding lands channels the northern continental winds and generate a sheared wind system on the shelf (Figure 1) : Mistral landwind (channelled between Alps and Massif Central mountains) and Tramontane landwind (channelled between Massif Central and Pyrenees mountains) may blow together or separately, and generate highly variable curl patterns on the shelf, resulting in very intermittent shelf circulation [Estournel et al., 2003].

One major challenge for long term coastal modeling is the availability of atmospheric forcing fields which are able to drive such complex and fine scale coastal dynamics. The resolution in space and time of the forcing data sets is an important requirement to obtain realistic results. Hereafter, we present numerical results obtained with “realistic” coastal modelling. The aim is to underline the impact of the resolution of the atmospheric forcing in a shelf area like the Gulf of Lions. The analysis focuses on the fine scales and intermittent processes and on their impact on the thermodynamical state of the ocean at short but also at long time scales.

High resolution coastal model

Ocean model

The circulation model is based on NEMO [Madec et al., 2008] and is designed to study the physical processes at the shelf edge during a quasi-climatic period of 11 years (1990-2000).

The coastal and shelf sea model configuration (named GoL64) covers the Gulf of Lions continental shelf (see Figure 1) with a horizontal resolution of 1/64° on a regular Mercator mesh (~ 1.25×1.25 km²). This resolution allows to explicitly resolving the mesoscale dynamics (the internal Rossby deformation radius is around 3 km on the shelf). In a Cartesian coordinate level model such as NEMO, the mixed layer depth varies level by level. Thus, a high resolution in the upper ocean is recommended in order to accurately represent the mixed layer processes. Bernie et al. [2005] showed that in order to resolve 90% of the observed SST variability, a vertical resolution of at least 1m is required in the upper ocean. In our study, the vertical resolution uses 130 z-levels, spaced out by 1 m from the surface to about 35 m depth, and by no more than 30 m near the bottom. The diurnal mixed layer and the seasonal thermocline are then well sampled, allowing a precise study of their structure. The bottom topography is represented by partial cells which contour in an optimal way the abrupt shelf break.

Conditions at the limits of the regional model are handled by radiative open boundary conditions and are using data provided every 5 days by a hindcast of the ocean circulation carried out with a high resolution (1/16°) ocean circulation model of the whole Mediterranean Sea driven by ERA40 [Uppala et al. 2005] atmospheric reanalysis. Initial conditions are also derived from this simulation.

Atmospheric forcing

For global ocean models, the spatial resolution of global atmospheric reanalyses [NCEP or ERA40] allows a coherent coupling. For coastal and shelf seas modelling, regional atmospheric reanalyses become essential. Temporally, a diurnally varying atmospheric forcing is required to represent high frequency ocean processes. Bernie et al. [2005] showed that a temporal resolution of the surface fluxes of 3h or less is necessary to study the variations of SST.

The present study uses the surface atmospheric parameters provided by a dynamical downscaling of ECMWF global data (ERA15 reanalysis and ECMWF analyses) with the regional atmospheric climate model REMO [Jacob et al., 2001]. The REMO atmospheric dataset has a horizontal resolution of 1/6° (~ 18 x 18 km²) which allows the description of local particularities of the wind-system, and an hourly temporal resolution which allows a representation of the diurnal cycle and of the intermittency of the winds. Details and references about the physical parameterisations can be found in Jacob et al. [2001]. An evaluation of the REMO regional reanalysis in the Gulf of Lions over the period 1990-2000 has been performed by Langlais et al. [2009a].

To evaluate the benefit of the high spatial and temporal resolution of the REMO dataset, three simulations has been run:

- GoL64. This simulation is driven by the REMO hourly forcing. It is considered as the reference since the forcing has both high spatial (18 km) and temporal (1 hour) resolution.
- GoL64-ERA40. This simulation is driven by the 6 hourly forcing obtained from the ERA40 reanalysis [Uppala et al., 2005]. This simulation is compared to GoL64 to assess the effect of the spatial resolution since the horizontal resolution of ERA40 is 125 km.
- GoL64-DAY. This simulation is driven by the REMO daily forcing obtained by averaging the hourly forcing over 24 hours. It is used to assess the impact of resolving the diurnal cycle of the atmospheric forcing.

Impact of the forcing spatial resolution

In the Gulf of Lions, the continental influence (the shape of the shelf, the coastline, the local orography) constrains the spatial distribution of the atmospheric fields. In situations dominated by continental winds, the fine resolution of REMO atmospheric forcing produces much more realistic wind patterns, with a clear separation of the flows corresponding to the two dominant wind systems, the Tramontane and the Mistral. Differently, ERA40 proposes a rather uniform northerly wind (Figure 2). The representation of the wind curl patterns, of the sheltered areas, and of the off shore distribution of air-sea fluxes are consequently very different, with finer patterns and a better definition of gradients in the offshore direction with the REMO winds (GoL64 run). Wind speeds are also significantly greater in REMO.

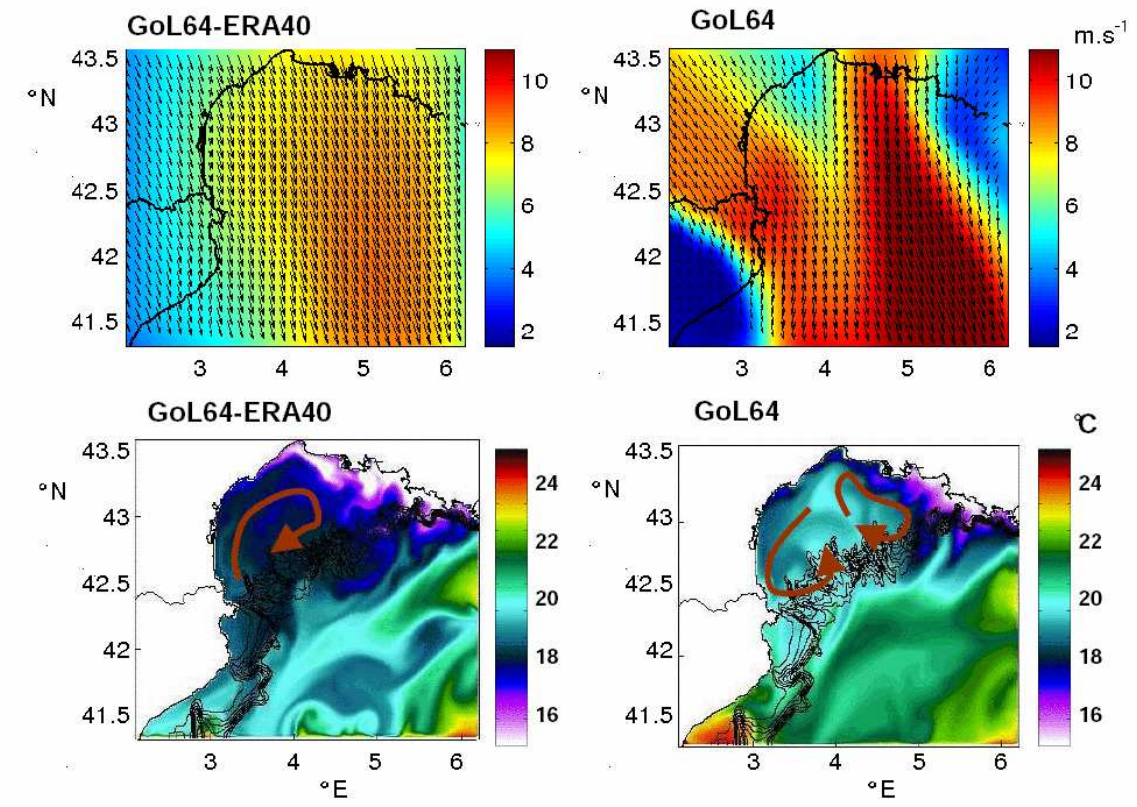

Figure 2

Comparison between the GoL64 and GoL64-ERA40 runs at the same date (8th July 1990) under a continental weather regime. Upper panels compare ERA40 (left panel) and REMO (right panel) wind fields. Lower panels represent the SST fields, the red arrows marking a schematic of the mean currents.

These differences in the representation of the major wind systems have drastic consequences on the ocean shelf circulation and hydrology, as shown in figure 2. The uniform northerly wind system of ERA40 induces a large anticyclonic circulation on the shelf, whereas the separation of the Mistral and Tramontane wind systems in REMO generates a double gyre circulation, cyclonic in the western part of the shelf and anticyclonic in the East. Between these two circulation cells, the convergence of the flow drives intrusions of warm waters of the slope current into the central part of the shelf. The impact on the shelf water temperature is noticeable, shelf waters being significantly warmer in the GoL64 run. The better resolution of the details of the wind field in REMO also improves the strength and the representation of the coastal upwellings, the distribution of which is much more fragmented with REMO forcing, in agreement with the observations of Millot [1990], whereas the ERA40 forcing produces a rather uniform upwelling along the coast.

Impact of the temporal resolution

The diurnal cycle of the atmospheric forcing generates high frequency processes which are energetic and ubiquitous features of the ocean circulation in the Gulf of Lions. The impact of the hourly resolution does not only concern the dynamics, but also the thermal structure and the heat content of the upper ocean.

High frequency ocean processes and vertical mixing

Resolving the diurnal cycle in the atmospheric forcing enhances the realism of the model solution. The diurnal cycle of the heat fluxes generates a diurnal mixed layer. The hourly variations of the wind reproduce a sea-land breeze forcing at the sea surface and more frequent stronger and intermittent wind extremes. The ocean response is then energetic oceanic oscillating motions in the diurnal-inertial frequency band. The wind bursts are also shown to erode the stratification and to induce internal inertial waves that can be felt at depth greater than 50 m.

In a microtidal area like the Gulf of Lions, motions in the diurnal-inertial band are the dominant mechanisms for vertical exchange through a stratified water column [Pollard et al., 1973; Simpson et al., 2002]. The energetic high frequency features play the role of destabilisation forces which erode the stratification. They modify the turbulence level and lead to a significant increase of the vertical mixing in the first 20 meters. This is shown in figure 3 which compares the time-depth evolution of vertical mixing coefficient in GoL64 and GoL64-DAY runs during a 29 day period in summer.

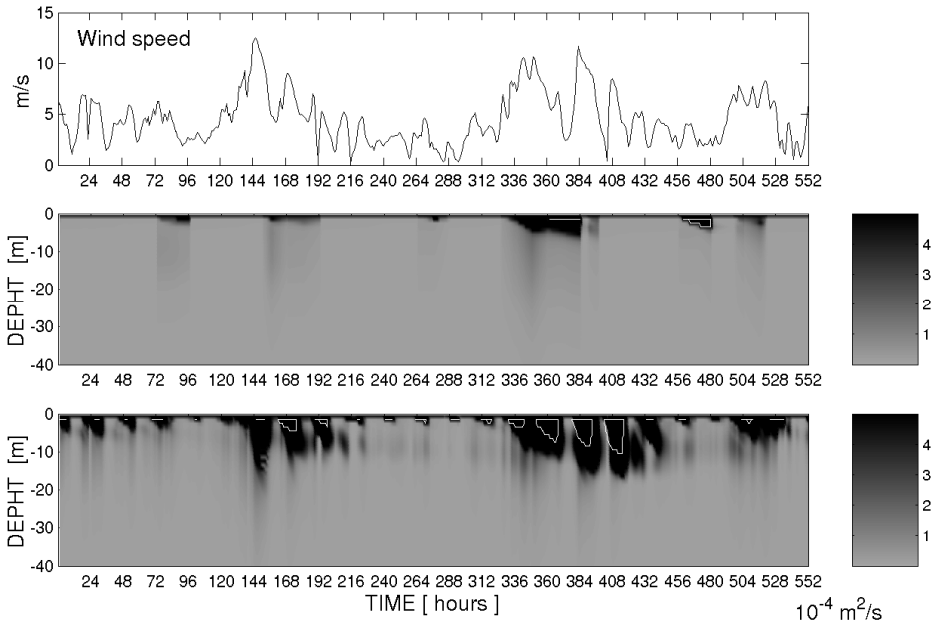

Figure 3

10 meters wind speed (top), time-depth variations of the vertical eddy coefficient (in 10-4 m2/s) in run GoL64-DAY (middle), and in run GoL64 runs (bottom). The grey palette is saturated at 5.10-4 m2/s. The white lines underline the 10 m2/s contour (which corresponds to the activation of the convection parameterization). Horizontal time axis ranges from 1 to 552 hours (~29days).

In NEMO, the parameterization of the vertical mixing uses a modified TKE closure scheme [Madec, 2008] which can produce a realistic mixed layer structure on high resolution grid [Chen et al., 1994]. All the high frequency processes do not have the same impact on the calculation of the eddy vertical mixing. The direct impact of the wind strongly and deeply constrains the vertical mixing coefficient calculation. The wind bursts induce erosion of the thermocline and homogenization of the water column. Deep peaks of strong vertical diffusion coefficients mark the impact of the wind stirring in figure 3. The introduction of a diurnal mixed layer has also an important impact on the calculation of the eddy vertical coefficient. Diurnal temperature variations modify the behaviour of the turbulent layer: they enhance vertical mixing at night and can limit the mixing during the day (when medium winds occur (less than 5m/s)). So a diurnal variation of the vertical mixing coefficient is shown in figure 3. The association of night cooling and wind extremes leads to strong night convective events (marked with white lines) which homogenize the water column.

The enhanced mixing in run GoL64 results in a modification of the vertical distribution of heat in the upper ocean. A more intense vertical mixing leads to deeper heat propagation (Figure 4) which is characterized by a cooling of the surface layer and a warming of the layers between 10 and 30 meters.

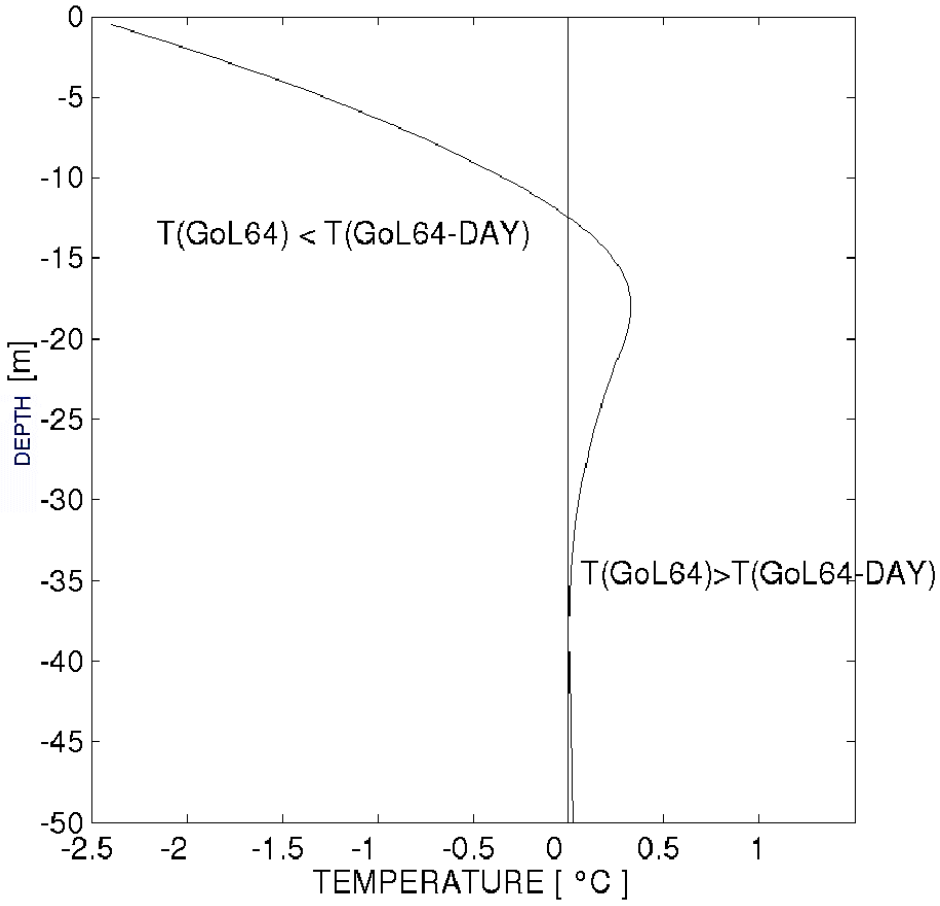

Figure 4

Mean temperature profile differences between the two runs: GoL64 - GoL64-DAY.

Air-sea fluxes and thermal content

Resolving the diurnal cycle of the atmospheric forcing introduces diurnal variations of SST, a crucial parameter for air-sea fluxes calculation [Fairall et al. 1996; Schiller and Godfrey, 2005; Ward, 2006]. In NEMO, the air-sea fluxes that drive the model are calculated with bulk formulae [Large, 2006; Large and Yeager, 2008]. The model SST is used to calculate the turbulent heat fluxes and the upward longwave radiation. The diurnal variations of SST modify the temporal mean of those fluxes. In the case presented here (between July 18 and August 15 in 1990) these SST variations reduce the net ocean heat gain by 30 W/m2 in average over the period (Table 1), mainly because of an increase of evaporation. This non-negligible effect limits the summertime warming of the ocean. Spatially the effect is homogeneous, and after 29 days the upper ocean temperature (52 first meters) of the run driven by the hourly forcing is 0.35°C cooler than the upper ocean temperatur e of the run driven by daily averaged forcing.

Heat Fluxes gained by the ocean in W/m²	***Sensible Flux***	***Latent Flux***	***Upward longwave flux***	***Net heat flux***
GoL64-DAY run	5.96	-29.64	-70.60	167.67
GoL64 run	3.43	-51.62	-66.39	135.04

Table 1

29 day mean values of the sensible and latent heat fluxes (W/m2), of the upward longwave radiation and of the net surface heat flux, for the runs GoL64-DAY and GoL64.

Integrated effect and climatic impact

In the long term, the mean state and the interannual variability of the circulation and hydrology on the shelf is the result of the integration over time of the interaction of the processes previously described. The intermittent and fine scale processes not only modify instantaneous behaviours but may have significant impact at climatic scales.

Discussion of long term impact

The analysis of the diurnal cycle has been performed during a summer period. The diurnal variations of SST have been shown to modify the heat budget in a significant way. The cooling effect of 30 W/m2 over a full summer month is higher than the uncertainties of the air-sea fluxes (~ 10 W/m2). It should be interesting to study the impact of the diurnal variations of the SST during a multi-year simulation, to evaluate its effects during the subsequent winter period and in the long-term.

In the Gulf of Lions, strong convective events occur during wintertime on and off the shelf, the intensity of which depends on the preconditioning of the stratification of the water column that occurs during summer and fall. In run GoL64, a cooler net heat flux and stronger heat propagation at depth weaken the stratification in the first 20 meters, but enhance it between 20 and 30 meters (Figure 5). The modification of the stability of the water column may then modify winter deep convective events.

Moreover, the wind bursts probably have a strong impact on the convective events during the winter periods, increasing the evaporation and the turbulence level. The shelf dense water formation and export are studied in more detail in the next section.

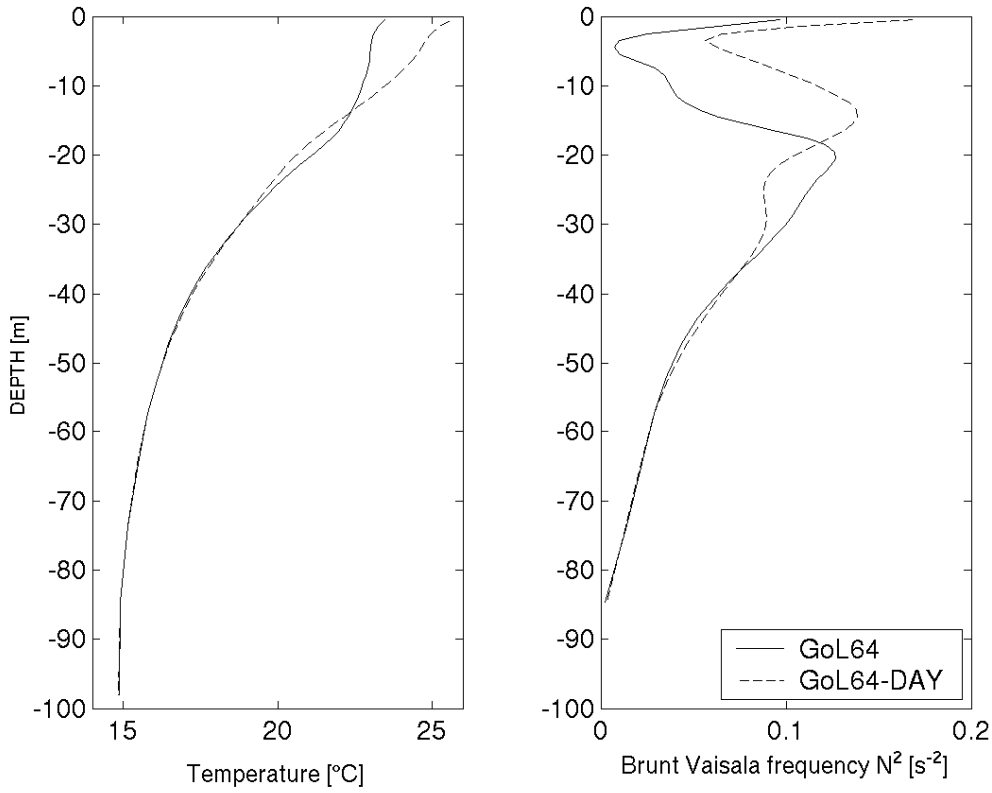

Figure 5

Stability of the water column. GoL64 (black line) and GoL64-Day (black dotted line) temperature profiles (left panel) and Brunt Vaisala frequency (right panel) of the day 29.

Example of the shelf dense water

Dense waters formed on the shelf contribute to the exchanges between the shelf and the open ocean when they cascade down the shelf break, as canyons in the shelf break channelling dense water plumes to greater depth. Bursts of exported dense shelf waters in canyons have been shown to be favoured by extreme wind events [Langlais, 2007]. In the Gulf of Lions, the western end of the shelf break is known as an important pass for the shelf/open-ocean exchanges [Dufau-Julliand et al., 2004]. A 3D representation of the shelf dense water is presented in figure 6, during a strong wind event which lasts a few days at the end of

February 1991. Each picture represents the strongest export of dense shelf water during this period (on the 23rd of February in the simulation driven by the ERA40 6-hourly forcing, and on the 26th of February in the simulation driven by the REMO hourly forcing). In the model, the characteristics of the shelf dense water are: S <38, T <13.5 and σ > 28.5. Those characteristics are warmer (and then lighter) than those find with in-situ measurements (S <38, T <12 and σ > 28.8) [Fieux, 1974; Dufau-Julliand et al., 2004]. The disagreement is mainly due to weak winter heat loss in REMO and ERA40: respectively -80 and -87 W/m2 instead of -100/-160 W/m2 [Bethoux et al. 2002].

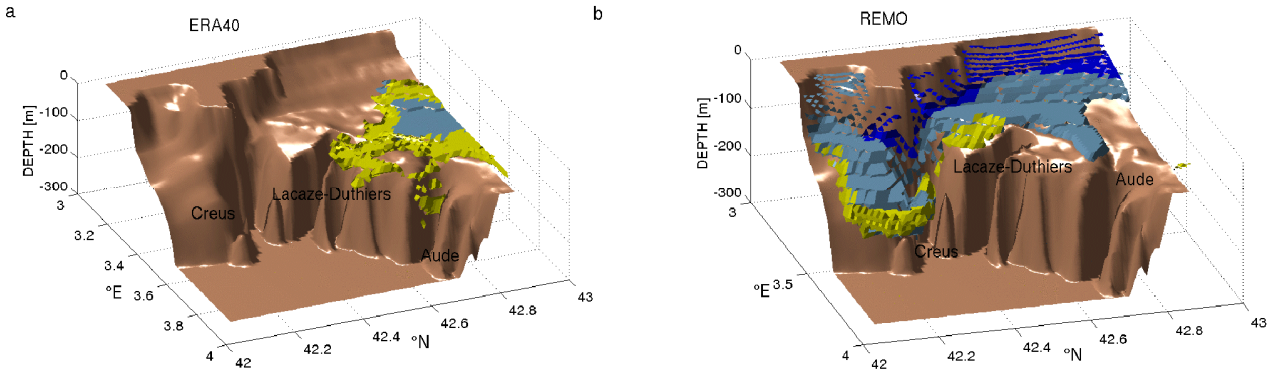

Figure 6

3D representation of the shelf dense water (characterized by S < 38, T < 13.5℃ and σ > 28.5) in (a) the GoL64-ERA40 run, and (b) the GoL64 run, during a strong wind event at the end of February 1991. Only the western part of the shelf break (which is broken by 3 major canyons, Creus, Lacaze-Duthiers and Aude) is represented and the bathymetry is shown until 300m. The dark blue underlines “cold” shelf dense water (T < 12.5℃), the blue underlines water between 12.5 and 13℃ and the yellow underlines “warm” shelf den se water (13 < T < 13.5℃).

During the storm, the REMO winds are strong enough to form shelf dense water on the shelf (the coldest water near the surface), and also to initiate the export of shelf dense water (previously formed and convected down to the shelf floor) through the Creus and Aude canyons in the GoL64 run. In GoL64-ERA40 run, the wind extremes are not strong enough during the storm: no dense water formation occurs near the surface during this period and shallow exports of relatively “warm” dense water are observed in the Lacaze-Duthiers and Aude canyons. As extreme winds bursts are less frequent and less marked in the ERA40 reanalysis, the formation and the export of “cold” dense shelf water through the canyon are rare in the GoL64-ERA40 run. Thus, the spatial and temporal resolution of the atmospheric forcing allows us to better simulate a crucial process involved in the exchanges at the shelf break. Since the shelf dense water contributes to the renewal of the Winter Intermediate Water, the resolution of the atmospheric forcing has also an important climatic impact on the water masses.

Conclusion

The atmospheric forcing drives fine scale processes involved in the exchanges at the shelf break in the Gulf of Lions. The present model study demonstrates in a quantitative way that a high spatial and temporal resolution of the atmospheric forcing is an absolute requirement to simulate the complex shelf dynamics in a realistic way [Langlais et al. 2009a].

The high frequency timescales are not often taken into account in the forcing of ocean models, but they control energetic and omnipresent features of the upper ocean which are able to constrain the long-term variations of the thermodynamical state of the upper ocean [Langlais et al. 2009b].

Coastal modeling is an actual challenge for the operational oceanography as well as climatic studies. Thanks to the international ocean community effort within GODAE (Global Ocean Data Assimilation Experiment) and the following projects like MyOcean in the framework of the European Marine Core Services, open ocean boundaries conditions are and will be available for almost any coastal area. A future challenge will be to provide the suitable atmospheric forcing.

Acknowledgements

The authors wish to thank the support from Ministère de l'Education nationale et de la Recherche and from Centre National de la Recherche Scientifique. We acknowledge the support from the French national programme GMMC and from the national centre for computational resources IDRIS. This work has been part of the DRAKKAR project and the LEFE IDAO project.

References

Albérola C., Millot C., and Font J. 1995: On the seasonal and mesoscale variabilities of the northern current during the PRIMO-0 experiment in the western Mediterranean Sea. Oceanologica Acta, 18(2):163-192.

Bethoux J., Durrieu de Madron X., Nyffeler F., Tailliez D., 2002: Deep water in the Western Mediterranean: peculiar 1999 and 2000 characteristics, shelf formation hypothesis, variability since 1970 and geochemical inferences. Journal of Marine Systems, 33-34:117-131

Bernie, D. J., Woolnough S. J., Slingo J. M and Guilyardi E. 2005: Modeling of diurnal and intraseasonal variability of the ocean mixed layer. J. Climate, 18:1190–1202.

Chen D., Rothstein L.M. and Busalacchi A.J., 1994: A hybrid vertical mixing scheme and its application to tropical ocean models. Journal of Physical Oceanography, 24:2156-2179.

Dufau-Julliand C., Marsaleix P., Petrenko A., Dekeyser I. 2004: Three-dimensional modeling of the Gulf of Lions' hydrodynamics (northwest Mediterranean) during january 1999 (MOOGLI3 experiment) and late winter 1999: Western Mediterranean Intermediate Water's (WIW's) formation and its cascading over the shelf break. Journal of Geophysical Research, 109C11002, doi:10.1029/2003JC002019.

Estournel C., Durrieu de Madron X., Marsaleix P., Auclair F., Julliand C., Vehil R. 2003: Observation and modelisation of the winter coastal oceanic circulation in the Gulf of Lions under wind conditions influenced by the continental orography (FETCH experiment). Journal of Geophysical Research, 108(C3)8059, doi:10.1029/2001JC000825.

Fairall C. W., Bradley E. F., Godfrey J. S., Wick G. A., Edson J. B. and Young G. S. 1996: Cool-skin and warm-layer effects on sea surface temperature. J. Geophys. Res., 101:1295–1308.

Fieux, M. 1974: Formation d'eau dense sur le plateau continental du Golfe du Lion. Colloques Internationaux du CNRS N215. 165-174.

Flexas M., Durrieu de Madron X., Garcia M., Canals M., Arnau P. 2002: Flow variability in the gulf of lions during the mater HFF experiment (March-May 1997). Journal of Marine System, 33-34:197-214.

Huthnance J.M. 2002: Wind-driven circulation in coastal and marginal seas. Canadian Journal of Remote Sensing, 28:329-339.,

Jacob D., Andrae U., Elgered G., Fortelius C., Graham L.P., Jackson S.D., Karstens U., Koephen C., Lindau R., Podzun R., Rockel B., Rubel F., Sass H.B., Smith RND., Van den Hurk BJJM.,Yang X. 2001: A comprehensive Model Intercomparison Study Investigating the Water Budget during the BALTEX-PIDCAP Period. Meteorology and Atmopsheric Physics, 77, issue 1-4, 19-43.

Johns B., Marsaleix P., Estournel C., Vhil R. 1992: On the wind-driven coastal upwelling in the Gulf of Lions. Journal of Marine Systems, 3:309-329.

Langlais C., 2007. Etude de la variabilité interannuelle des échanges côte-large : simulation haute résolution de la dynamique du Golfe du Lion. PhD thesis of the Toulon Var University.

Langlais C., Barnier; B., Molines J-M, Fraunié P., Jacob D. and Kotlarski S. 2009a: Evaluation of a dynamically downscaled atmospheric reanalysis in the prospect of forcing long term simulations of the ocean circulation in the Gulf of Lions. Submitted to Ocean Modelling.

Langlais C., Barnier B., Fraunie P. and Schiller A. 2009b: Resolving the diurnal variability of atmospheric forcing in a coastal ocean circulation model of the Gulf of Lions (NW Mediterranean): impact on the thermodynamical state of the upper ocean. Submitted to Ocean Modelling.

Large, W.G. 2006: Surface fluxes for practitioners of global ocean data assimilation, J.Verron and E.Chassignet, Edition.Springer, Dordrecht, the Netherlands, 229-270.

Large, W. G., Yeager S.G., 2008: The global climatology of an interannually varying air-sea flux data set. Climate Dynamics, doi:10.1007/s00382-008-0441-3.

Madec, G., 2008. NEMO Ocean General Circulation Model Reference Manuel. Internal Report, LODYC/IPSL, Paris.

Mertens C., Schott F. 1998: Interannual variability of deep-water formation in the Northwestern Mediterranean. Journal of Physical Oceanography, 28:1410-1424.

Millot C. 1979: Wind induced upwellings in the Gulf of Lions. Oceanologica Acta, 2(3):261-274

Millot, C. 1990: The Gulf of Lions' hydrodynamics. Continental Shelf Research 10(9-11), 885-894.

Millot C. and Crépon M. 1981. Inertial oscillations on the continental shelf of the Gulf of Lions - Observations and theory. Journal of Physical Oceanography, 11(5):639-657.

Pollard R.T, Rhines P. B., and Thompson R. O. R. Y. 1973: The deepening of the wind-mixed layer. Geophys. Fluid Dyn., 3:381–404.

Reffray G., Fraunié P. and Marsaleix P. 2004: Secondary flow induced by wind forcing in the Rhône region of freshwater influence. Ocean Dynamics, 54:179-196.

Schiller, A. and Godfrey J. S., 2005: A diagnostic model of the diurnal cycle of sea surface temperature for use in coupled ocean-atmosphere models. Journal of Geophysical Research, 110, C11014, doi:10.1029/2005JC002975

Shapiro G., Huthnance J. and Ivanov V. 2003: Dense water cascading off the continental shelf. Journal of Geophysical Research, 108(C12)3390, doi:10.1029/2002JC001610.

Simpson J.H. 1997: Physical processes in the ROFI region. Journal of Marine Systems, 12:3-15.

Simpson J.H., Hyder P., Rippeth T.P. and Lucas I.M. 2002: Forced Oscillations near the Critical Latitude for Diurnal-Inertial Resonance. Journal of Physical Oceanography, 32:177-187.

Uppala S.M., Kallberg P.W., Simmons A.J., Andrae U., da Costa Bechtold V., Fiorino M., Gibson J.K., Haseler J., Hernandez A., Kelly G.A., Li X., Onogi K., Saarinen S., Sokka N., Allan R.P., Andersson E., Arpe K., Balmaseda M.A., Beljaars A.C.M., van de Berg L., Bidlot J., Bormann N., Caires S., Chevallier F., Dethof A., Dragosavac M., Fisher M., Fuentes M., Hagemann S., Holm E., Hoskins B.J., Isaksen L., Janssen P.A.E.M., Jenne R., McNally A.P., Mahfouf J-F., Morcrette J-J., Rayner N.A., Saunders R.W., Simon P., Sterl A., Trenberth K.E., Untch A., Vasiljevic D., Viterbo P. and Woollen, J., 2005: The ERA-40 re-analysis. Quarterly Journal of the Royal Meteorological Society, 131:2961-3012.

Van Haren H. and Millot C., 2003. Seasonality of internal gravity waves kinetic energy spectra in the ligurian basin. Oceanologica Acta, 26:635-644.

Ward B. 2006: Near-surface ocean temperature. Journal of Geophysical Research, 111, C02005, doi:10.1029/2004JC002689.

Ocean circulation in the Mediterranean Sea: Input from Spatial Gravimetry

By Jean-Paul Boy[1,2], David Garcia[3], Scott B. Luthcke[2], David D. Rowlands[2], Douglas S. Chinn[4]

[1] EOST - IPG (UMR 7516 CNRS-ULP), Strasbourg, France.
[2] NASA Goddard Space Flight Center, Greenbelt, USA.
[3] Dpto. Matematica Aplicada, Universidad de Alicante, Espagne.
[4] SGT Inc.@ NASA Goddard Space Flight Center, Greenbelt, USA.

Abstract

We derive mass variations at sub-basin scale in the Mediterranean and Black Seas from the GRACE (Gravity Recovery And Climate Experiment) inter-satellite K-band range-range (KBRR) data for the period April 2003 to September 2007, using a localized surface mass concentration (mascon) parameterization. We compare these observed mass variations to the North-Atlantic and Mediterranean Sea high resolution (PSY2V2) and global (PSY3V1) MERCATOR systems for a period of 2 years from September 2005 to September 2007. The PSY3V1 system is in better agreement with mass variations deduced from GRACE observations than the PSY2V2 system, despite its lower resolution (0.25° versus 0.067°) and the assimilation of only sea surface height from altimetry. Despite its limitation in spatial (a few hundreds of kilometres) and temporal (10 days) resolutions, time-variable gravity field recovered from the GRACE satellites appear to be an interesting independent validation tool for ocean models, which are already assimilating most of available oceanographic datasets (sea surface height and temperature, as well as temperature and salinity profiles).

Introduction

Thanks to the launch of the GRACE mission in April 2002, Earth's time variable gravity field is now recorded with unprecedented precision and spatial resolution (see Tapley et al., 2004a). The mission consists of two satellites in near polar orbits, flying at approximately 500 kilometres, and 250 kilometres apart. The distance between the two spacecrafts is measured precisely through a microwave (K-band) ranging system. In addition, the orbit of each satellite is monitored using GPS (Global Positioning System) receivers and attitude sensors, as well as high-precision accelerometers.

The global circulation of surface geophysical fluids (atmosphere, oceans, continental water storage, etc.) induces global mass redistribution, and therefore gravity field variations. The main objective of the GRACE mission is indeed the monitoring of mass variations at the Earth's surface, i.e. continental hydrology, ice sheets and oceanic variations. The classical spatial and temporal resolutions allowed by the classical spherical harmonic solutions are typically 400 kilometres and a week to one month respectively (see, for example, Tapley et al., 2004a, 2004b and Wahr et al., 2004).

Although oceanic mass variations are usually one order of magnitude smaller than the contributions from continental hydrology (see, for example, Syed et al., 2008) and ice sheets (Velicogna and Wahr, 2005; Luthcke et al., 2006; Llubes et al., 2007), GRACE accuracy allows the detection of small amplitude oceanic mass changes, equivalent to a few centimetres of equivalent water height (see, for example, Munekane, 2007). However, only large-scale mass variations can be studied using the spherical harmonic solutions (see, for example, Chamber and Willis, 2008).

Thanks to several decades of radar altimetry, sea surface height variations are monitored, in almost real time, with a precision of about 1 centimetre. They can be decomposed into i) mass-induced variations (due to changes in fresh water input, for example), which can be recovered from GRACE, and ii) steric expansion (due to temperature and to a smaller extend salinity variations). When looking at seasonal, but also at longer timescales, mass and volume variations can be significantly different (see Lombard et al., 2005, regarding the contribution of thermal expansion on mean sea level rise).

Moreover, GRACE recovers mass variations that can be used as a validation technique of ocean general circulation models; as most of oceanographic datasets (sea surface height and temperature, in-situ measurements of temperature and salinity, etc.) are nowadays assimilated into ocean models, such as MERCATOR, only other independent measurements can be used for validation. However, because GRACE data are not processed in real-time, space gravity can only be used a posteriori, or to validate reanalysis-type products.

There are several reasons to study inferred mass changes preferentially in the Mediterranean Sea:

- As shown by Garcia et al. (2006), seasonal sea surface height variations are out-of-phase of seasonal mass changes. Sea level maximum is reached in summer, due to thermal expansion, when mass variations reach its lowest, due to evaporation. Amplitudes of mass variations in the Mediterranean Sea are among the largest over the entire oceans.

- The Mediterranean Sea has recently experienced significant changes in its circulation, and not only at its surface (see, for example, Vigo et al., 2005).
- The first eddy-resolving operational model developed by the MERCATOR project was focused on the North Atlantic Ocean and the Mediterranean Sea.

After a quick description of our GRACE regional solution over the Mediterranean and Black Seas, we present the comparison of mass variations recovered from space, to mass variations computed from two operational MERCATOR systems PSY2V2 and PSY3V1.

GRACE mascon solutions for the Mediterranean and the Black Seas

Monthly (or sub-monthly) time-variable gravity solutions from the GRACE mission are usually expressed in terms of global spherical harmonics. Mass variations within a defined area are then computed using an averaging kernel, as defined by Swenson and Wahr (2002). In this approach, the monthly Stokes coefficients of the gravity field are first estimated directly from the GRACE level-1 tracking data (as a level-2 product). The mass flux is then derived as a level-3 product in a second step. In the course of this second step, the original level-2 product is altered by the required smoothing.

We use a different approach where mass flux is estimated as a level-2 product directly from GRACE level-1 tracking data as in Rowlands et al. (2005). Our level-2 products are mass concentration parameters (mascons). Each mascon parameter is actually estimated as a scale factor on a set of lumped Stokes coefficients. In this approach, individual Stokes coefficients are very well constrained and no-post solution smoothing is required. Spatial and temporal constraints are combined in the solution for mascons together with GRACE tacking data and enable increased spatial and temporal resolution. For example, Luthcke et al. (2006) were able to observe Greenland ice sheet ice mass loss in all the different major drainage basins, unlike early studies using spherical harmonic gravity fields (see, for example, Velicogna and Wahr, 2005). Using the same technique, Luthcke et al. (2008) were able to separate mass variations from individual glaciers in Alaska, unlike other studies using spherical harmonic solutions (Chen et al., 2006). We therefore choose to adopt this methodology in order to retrieve mass variations in the Mediterranean and Black Seas, which have been divided into 10 different blocks (see Figure 1). The blocks in the Mediterranean Sea generally correspond to the areas with different sea surface height and temperature trends, as observed by Vigo et al. (2005).

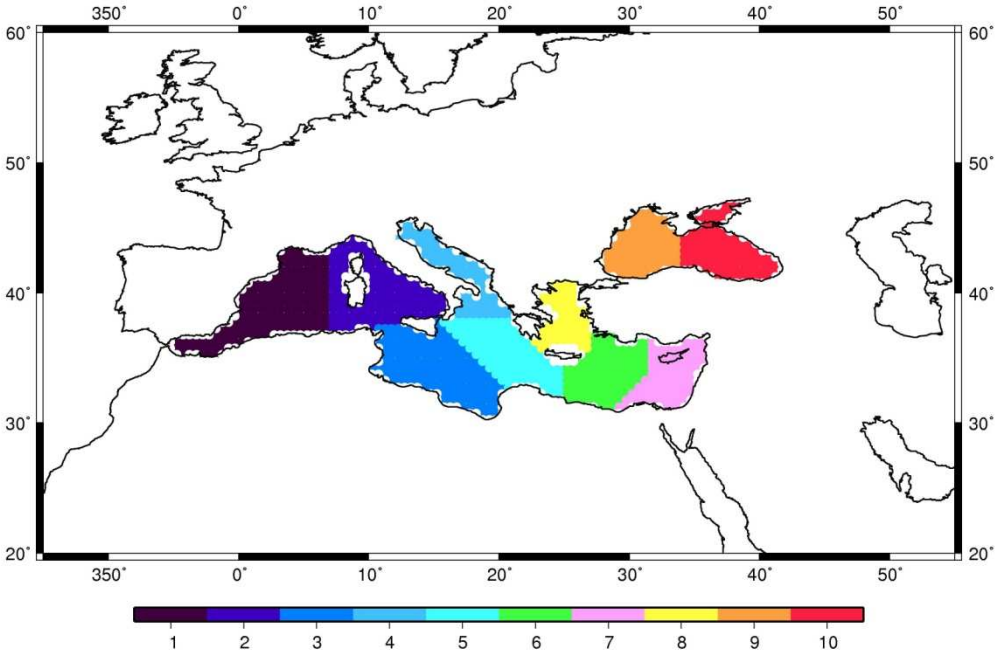

Figure 1

Definition of the 10 mascon cells over the Mediterranean and Black Seas

The recovery of oceanic and hydrological contributions in GRACE KBRR (K-band range-rate) requires precise accounting of the other sources of time-variable gravity field. We made solutions using two different forward modelling (v05 and v06) which includes:

- GOT4.7 ocean tidal model (Ray, 1999),
- Atmospheric time-variable gravity modelled up to degree and order 90, using 3-hourly pressure from ECMWF (European Centre for Medium-Range Weather Forecasts),
- High-frequency ocean time-variable gravity field modelled up to degree and order 90, using HUGO-m (Carrère and Lyard, 2003) barotropic ocean model, forced by 6-hourly ECMWF pressure and winds. This model is also used for high-frequency correction of sea surface height measurements from radar altimeters.
- For the v06 forward model only, time-variable gravity field due to terrestrial water storage variations is also modelled up to degree and order 90, using GLDAS/Noah (Rodell et al., 2004) 3-hourly soil-moisture, snow equivalent height and into water.

The v06 forward modelling ensures that the leakage of continental hydrology over the oceanic blocks is minimized (see Luthcke et al., 2006 and 2008 for more explanations).

Figure 2 shows 10-day mass variations in the Mediterranean and the Black Seas recovered from GRACE mascon solutions, using the v05 forward modelling (Luthcke et al., 2008) and 150 kilometre spatial constraints, from April 2003 to September 2007.

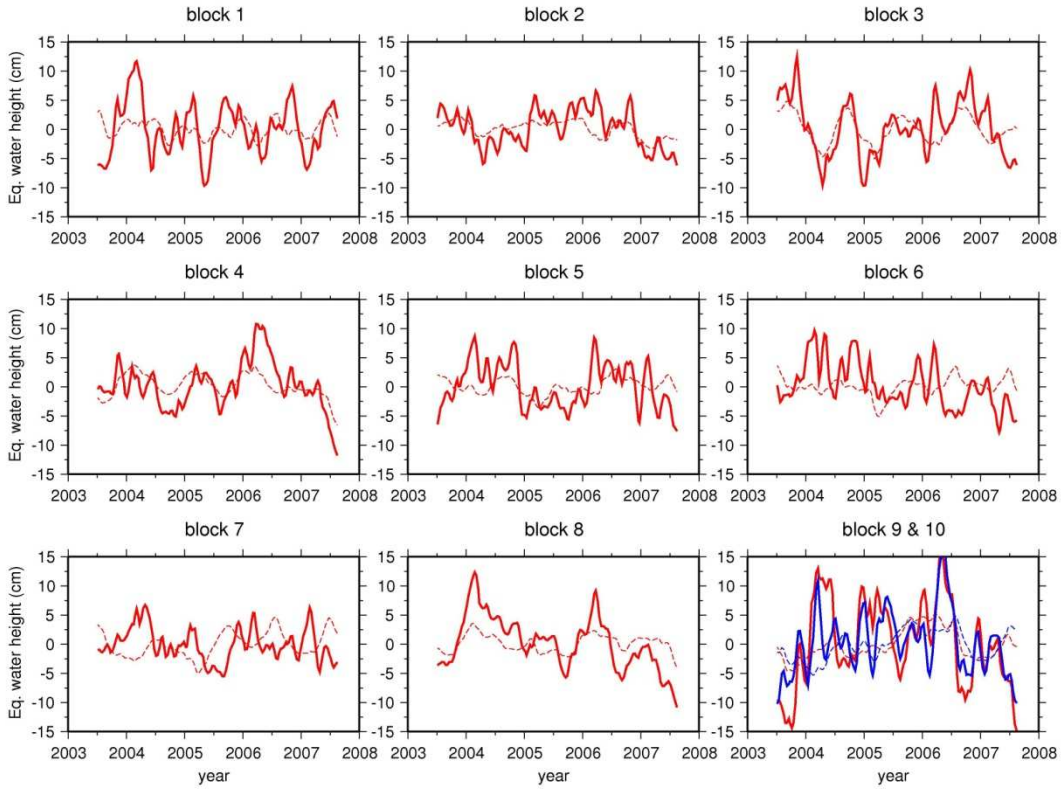

Figure 2

Mascon solutions (units: cm) (v05 forward model, and 150 km spatial constraints) over the Mediterranean Sea, expressed in terms of equivalent water height; The Western (block 9) and Eastern (block 10) Black Sea are respectively plotted in red and blue respectively. The differences between mascon solutions using v05 and v06 forward modelling are shown in dashed lines (units: cm).

As we are only interested in the oceanic mass variations, we choose to use the mascon solution with the v06 forward modelling, in order to avoid the contamination of continental hydrology into the ocean blocks. As continental hydrology is not modelled when using the spherical harmonic solutions from the GRACE project, it shows that our mascon approach and our different forward modelling are the only way to recover mass variations in the Mediterranean Sea at sub-basin scales, unlike previous studies by Fenoglio-Marc et al. (2006) and Garcia et al. (2006).

Comparison of GRACE mass variations and bottom pressure changes from MERCATOR models

We choose to compare oceanic mass variations recovered from the GRACE mission in the Mediterranean Sea to two following MERCATOR systems:

- The high resolution (1/15°) North-Atlantic and Mediterranean Sea run PSY2V2, which assimilates sea surface height from radar altimetry, sea surface temperature and profiles of temperature and salinity.
- The global (1/4°) run PSY3V1 which assimilated only sea surface height.

Because of its better spatial resolution, and the assimilation of temperature and salinity profiles, the high resolution model PSY2V2 should be more appropriate for describing mass changes in the Mediterranean Sea than the global PSY3V1 system.

GRACE solutions are related to mass variations, and are usually expressed in terms of equivalent water height. As the density of the ocean changes with depth and time, they can differ significantly from the sea surface height variations, as observed by radar altimetry.

We compute equivalent water height (i.e. mass variations) from daily temperature, salinity and sea surface height outputs in the Mercator PSY2V2 and PSY3V1 systems.

First, we estimate bottom pressure in (θ,λ) changes, computed from sea surface height variations $h(\theta,\lambda,t)$, and water density $\rho(\theta,\lambda,z,t)$ (reconstructed from temperature and salinity outputs at each level z):

$$p(\theta,\lambda,t) = \int_{-H(\theta,\lambda)}^{h(\theta,\lambda,t)} g\rho(\theta,\lambda,z,t)dz \qquad (1)$$

Where g and $H(\theta,\lambda)$ are the mean gravity at the Earth's surface and the bathymetry in (θ,λ).

They can be then converted to equivalent water height

$$\tilde{h}(\theta,\lambda,t) = \frac{p(\theta,\lambda,t)}{g\tilde{\rho}} \qquad (2)$$

Where $\tilde{\rho}$ is a reference density, taken as 1000 kg/m^3.

Figure 3 shows the RMS (root mean square) of the equivalent water height $\tilde{h}(\theta,\lambda,t)$ and sea surface height $h(\theta,\lambda,t)$ computed over a two-year period (2006/01 – 2007/12) for both PSY2V2 and PSY3V1 models.

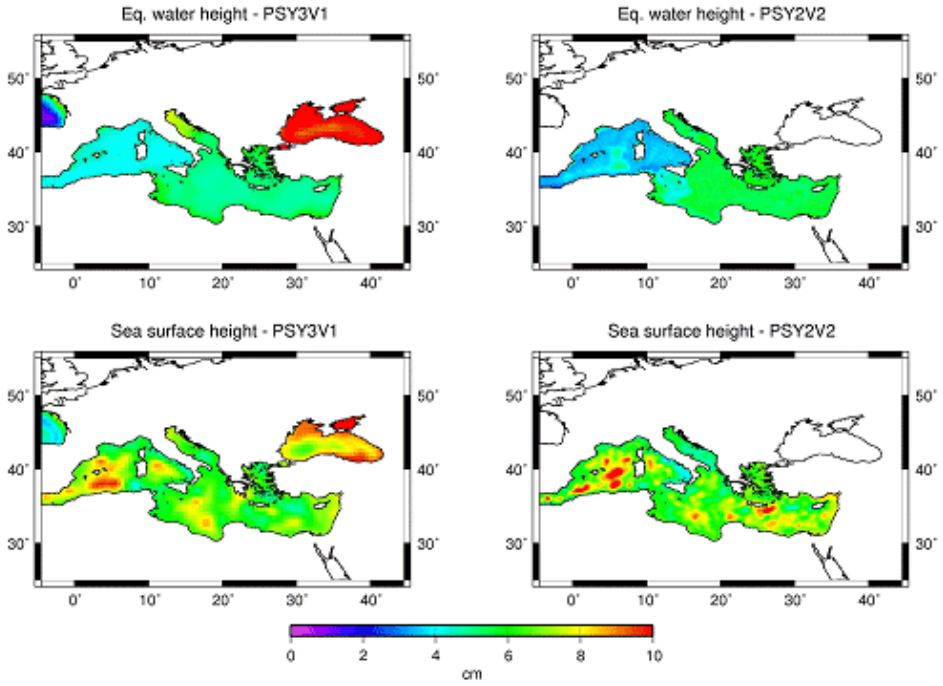

Figure 3

RMS of equivalent water height (mass) (units: cm) (tops panels) and sea surface height (volume) variations (units: cm) (lower panels), from PSY3V1 and PSY2V2 Mercator systems, computed for the 2006/01-2007/12 period.

Oceanic mass variations are usually smaller than sea surface height variability, especially at seasonal timescales, as only the latest are sensitive to thermal expansion, except for the Black Sea. Both PSY3V1 and PSY2V2 show smaller variations, in terms of equivalent water height, in the Western part of the Mediterranean Sea compared to the East.

Figure 4 shows the comparison between mass variations recovered from the GRACE mission (v06 forward modelling) and computed from PSY3V1 and PSY2V2 prototypes, for the 8 blocks in the Mediterranean Sea.

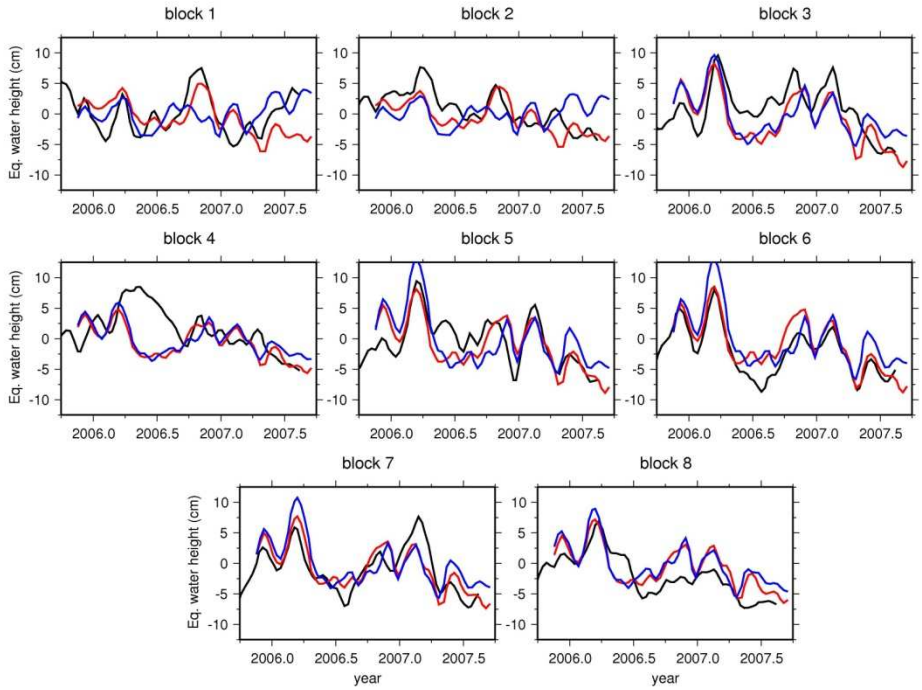

Figure 4

Comparison of GRACE mascon solutions (black) (units: cm) (v06) and equivalent water height (units: cm) derived from PSY3V1 (red) and PSY2V2 (blue) Mercator systems over the Mediterranean Sea.

Except for the first half of 2006, for the block 4 (Adriatic Sea), there is generally a good agreement between GRACE recovered mass variations and both MERCATOR prototypes. The Adriatic Sea block is relatively small, and is also surrounded by land, and might be therefore affected by hydrology leakage, as GLDAS/Noah (Rodell et al., 2004) does not model perfectly well continental water storage variations. There are also differences between the two MERCATOR runs, as the model configurations, the assimilation schemes and the assimilated data are different in the 2 systems.

As shown by the two models (Figure 3), mass variations deduced from GRACE observations show smaller variability in the Western Mediterranean Sea (Blocks 1 and 2), compared to the East and especially at seasonal timescales. The differences between PSY2V2 and PSY3V1 are also larger in this area.

In a more quantitative way, Table 1 gives the correlation coefficient between GRACE solutions (using both v05 and v06 forward modelling and mass variations computed from PSY3V1 and PSY2V2 prototypes)

	v05/PSY3V1	v05/PSY2V2	v06/PSY3V1	v06/PSY2V2
Block 1	0.2203	0.2605	**0.4095**	0.2473
Block 2	**0.6926**	-0.0181	0.5857	-0.0747
Block 3	0.4479	0.3259	**0.6055**	0.5242
Block 4	**0.3227**	0.2758	0.0775	0.0540
Block 5	0.5563	0.4445	**0.7385**	0.6424
Block 6	0.8993	0.8038	**0.9850**	0.8749
Block 7	0.7697	0.6902	**1.0508**	0.8371
Block 8	**0.7239**	0.6250	0.6653	0.5661
Block 9	**0.4537**		0.4354	
Block 10	0.3128		**0.4297**	

Table 1

Correlation coefficients between mass variations recovered from GRACE (v05 and v06 forward modelling) and computed from PSY3V1 and PSY2V2 MERCATOR prototypes. Bold numbers indicate the higher correlation for each block.

Despite its lower resolution and the assimilation of only sea-surface temperature, PSY3V1 derived mass variations are in better agreement with GRACE than PSY2V2 model. This result is quite surprising, as bottom pressure changes are sensitive to density variations, and as sea surface temperature, and temperature and salinity profiles from ARGO floats are assimilated in PSY2V2. These two models do not use also the same version of the NEMO (Madec et al., 1998) model (v8.1 and v8.2 respectively for PSY2V2 and PSY3V1). However, we do not have currently any explanation. It would be interesting to extend the comparison between GRACE and PSY2V2 and PSY3V1 models over the entire Northern Atlantic Ocean, in order to figure out if this conclusion is still valid.

Figure 5 shows the comparison between GRACE recovered mass variations (v06 forward modelling), equivalent water height (mass) and sea surface height (volume) for PSY2V2 prototype. As sea surface height variations from radar altimetry are assimilated in both PSY3V1 and PSY2V2 models, their average over each mascon blocks are much closer than the derived mass variations (Figure 4).

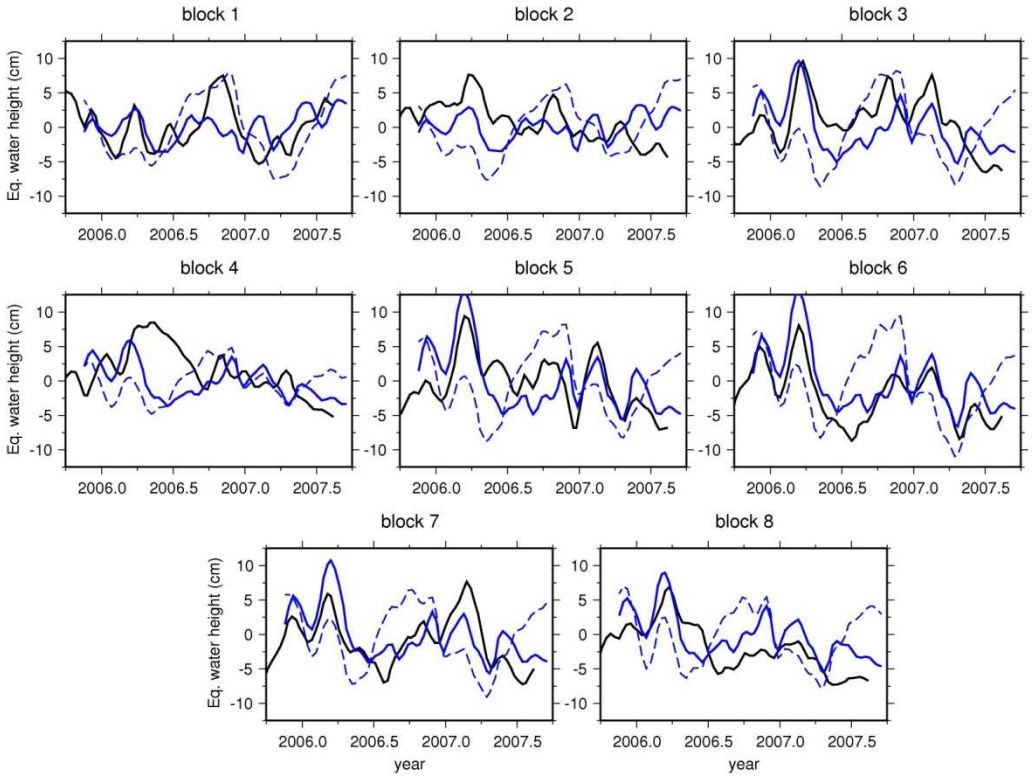

Figure 5

Comparison of GRACE mascon solution (black) (units: cm) and equivalent water height (blue) (units: cm) and sea surface height (dashed blue) (units: cm) from the Mercator PSY2V2 system in the Mediterranean Sea.

The case of the Black Sea is different. As the HUGO-m model used in the forward modelling does not include semi-enclosed seas, such as the Black Sea, our GRACE solution is not optimal. Also, the Black sea is only modelled with the PSY3V1 prototypes. However, we show on Figure 6, the comparison between our GRACE mascon solutions (blocks 9 and 10, using v06 forward modelling) and PSY3V1 derived equivalent water height.

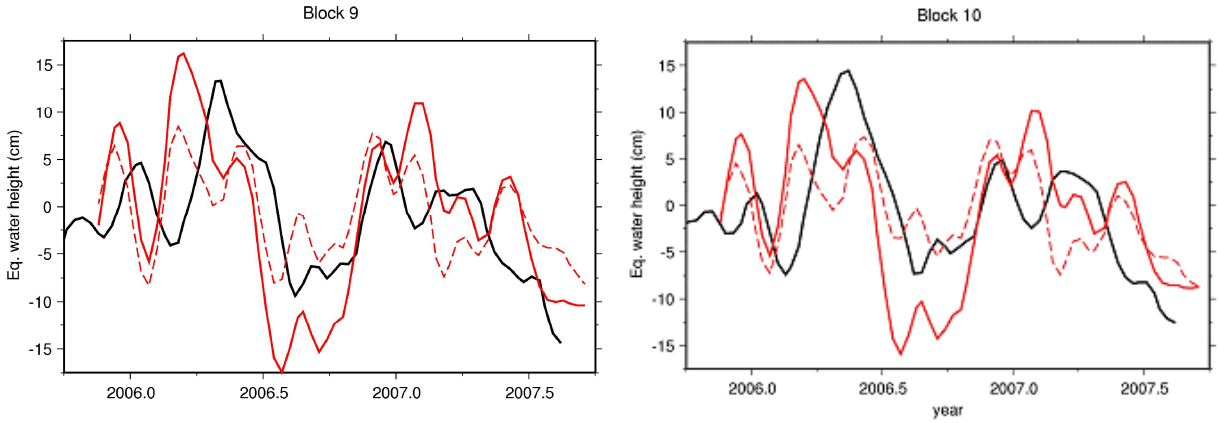

Figure 6

Comparison of GRACE mascon solutions (black) (units: cm), equivalent water height (red) (units: cm) and sea surface height (dashed red) (units: cm) from the PSY3V1 Mercator global system for the Black Sea.

Although the amplitude of GRACE and PSY3V1 mass variations are usually in agreement, there is indeed a significant phase lag, of about 1 month. We have currently no explanation. Our GRACE forward modelling can be however improved in this area, but the use of an updated version of the HUGO-m, with a higher temporal (3 hours) and spatial (0.25 degree) sampling, which also includes semi-enclosed basins, such as the Black Sea.

Discussion and conclusion

Oceanographers usually pay attention to the mean Earth's gravity field, as the mean dynamic topography (Rio and Hernandez, 2004) is obtained from the differences between mean sea surface (obtained from altimetry) and the geoid. However, since its launch in April 2002, time-variable gravity field, as recovered from the GRACE mission, allows nowadays the mapping of surface mass variations with a temporal resolution between typically 10 days and a month and spatial resolution of a few hundred to thousands of kilometers, depending on the processing strategies. As it allows increased both temporal and spatial resolutions, we analyze GRACE data using the mascon approach developed at NASA Goddard Space Flight Center (Rowlands et al., 2005; Luthcke et al., 2006).

Using this processing strategy, GRACE solutions are able to recover small wavelength (a few hundreds of kilometres) mass variations in the Mediterranean Sea, which are in good agreement with the bottom pressure modelled with PSY3V1 and PSY2V2 MERCATOR prototypes. Despite its lower resolution, and the assimilation of only sea surface height from radar altimetry, PSY3V1 prototype is in better agreement with GRACE than PSY2V2, although this model also assimilates sea surface temperature, and temperature and salinity profiles from ARGO floats.

It would be interesting, when GRACE data become available to compare PSY3V1 and PSY2V2 prototypes to their successors, i.e. PSY3V2 and PSY2V3, as they use a newer version of the OPA (v9, NEMO) model, as well as they assimilate both all available oceanographic datasets (sea surface temperature and height, temperature and salinity profiles). In addition, PSY3V2 uses another assimilation scheme (SEEK), instead of optimum interpolation.

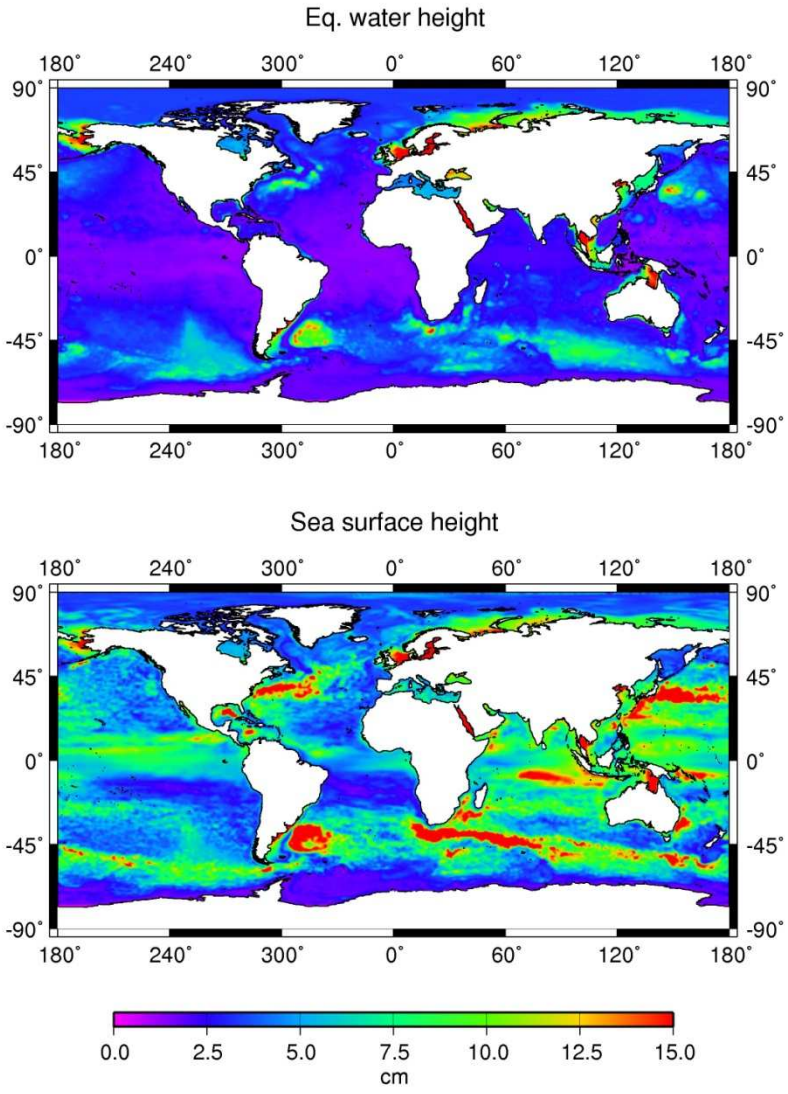

Figure 7

RMS variations of equivalent water height (cm) and sea surface height (cm), computed over a two year period (2006/01-2007/12) for the PSY3V1 Mercator global system.

This study over the Mediterranean and Black Seas should also be extended to the global ocean, although mass variations are not as large as in the Mediterranean Sea for most regions of the Earth. However, as shown by Figure 7, there are a few areas where equivalent water height root-mean-square variations are larger than 5 cm. The largest in terms of spatial extension is the Antarctic Circumpolar Current (Zlotnicki et al., 2007), other areas are the Argentina gyre, as well as the major mid-latitude currents (Gulf Stream and Kuroshio), which can only be modelled by eddy-resolving ocean general circulation models.

As time-variable gravity field data are generally not processed in near real-time, GRACE cannot be used as a validation tool for operational ocean models. However, as space gravimetry gives additional information about global mass redistribution, it could be used as one among the validation tools of reanalysis runs, such as the GLORYS (GLobal Ocean ReanalYses and Simulations) project.

Acknowledgements

Jean-Paul Boy is currently visiting NASA Goddard Space Flight Center, with a Marie Curie International Outgoing Fellowship (N°PIOF-GA-2008-221753). ***This work has been partially supported by the Spanish Ministry of Education and Science, research project ESP2006-11357***.

References

Carrère, C. and Lyard, F. 2003. Modeling the barotropic response of the global ocean to atmospheric wind and pressure forcing - Comparisons with observations. Geophys. Res. Lett., 30 (6), 1275, doi:10.1029/2002GL016473.

Chambers, D. P. and Willis, J. L. 2008. Analysis of large-scale ocean bottom pressure variability in the North Pacific. J. Geophys. Res., 113, C11003, doi: 10.1029/2008JC004930.

Fenoglio-Marc, L., Kusche, J. and Becker, M. 2006. Mass variation in the Mediterranean Sea from GRACE and its validation by altimetry, steric and hydrologic fields. Geophys. Res. Lett., 33, L19606, doi: 10.1029/2006GL026851.

Chen, J. L., Tapley, B. D. and Wilson, C. R. 2006. Alaskan mountain glacial melting observed by satellite altimetry. Earth Planet. Sci. Lett., 248 (1-2): 368-378.

Garcia, D., Chao B. F., Del Rio, J., Vigo, I. and Garcia-Lafuente, J. 2006. On the steric and mass-induced contributions to annual sea level variations in the Mediterranean Sea. J. Geophys. Res., 111, C09030, doi:10.1029/2005JC002956.

Llubes, M., Lemoine, J.-M. and Remy, F. 2007. Antarctica seasonal mass variations detected by GRACE, Earth Planet. Sci. Lett., 260: 127-136.

Lombard, A., Cazenave, A., Le Traon, P. Y., and Ishsii, I. 2005. Contribution of thermal expansion to present-day sea-level change revisited. Glob. Planet. Change, 47(1): 1-16.

Luthcke, S. B., Zwally, H. J., Abdalati, W., Rowlands, D. D., Ray, R. D., Nerem, R. S., Lemoine, F. G., McCarty, J. J. and Chinn, D. S. 2006. Recent Greenland ice mass loss by drainage system from satellite gravity observations. Science, 314, 1286 doi: 10.1126/science.1130776.

Luthcke, S. B., Arendt, A. A., Rowlands, D. D., McCarthy, J. J. and Larsen, C. F. 2008. Recent glacier mass changes in the Gulf of Alaska region from GRACE mascon solutions. J. Glaciol., 50 (188): 767-777.

Madec, G., Delecluse, P., Imbard, M. and Lévy, C. 1998. OPA8.1 Ocean general circulation model reference manual. Notes de l'IPSL, Université P. et M. Curie, B102 T15-E5, 4 place Jussieu, Paris cedex 5, N°11, 91p.

Munekane, H. 2007. Ocean mass variations from GRACE and tsunami gauges. J. Geophys. Res., 112, B07403, doi: 10.1029/2006JB004618.

Ray, R. D. 1999. A global ocean tide model from Topex/Poseidon altimetry: GOT99.2, NASA Tech Memo 209478, 58 pp.

Rio, M.-H. and Hernandez, F. 2004. A mean dynamic topography computed over the world ocean from altimetry, in situ measurements, and a geoid model. J. Geophys. Res., 109, C12032, doi: 10.1029/2003JC002226.

Rodell, M. et al. 2004. 2004. The Global Land Data Assimilation System. Bull. Amer. Meteor. Soc., 85 (3): 381-394.

Rowlands, D. D., Luthcke, S. B., Klosko, S. M., Lemoine, F. G. R., Chinn, D. S., McCarthy, J. J., Cox, C. M. and Andersen, O. B. 2005. Resolving mass flux at high spatial and temporal resolution using GRACE intersatellite measurements. Geophys. Res. Lett., 32, L04310, doi: 10.129/2004GL021908.

Swenson, S. and Wahr, J. 2002. Methods for inferring regional surface-mass anomalies from Gravity Recovery And Climate Experiment (GRACE) measurements of time-variable gravity. J. Geophys. Res., 107, B92193, doi: 10.1029/2001JB000576.

Syed, T. H., Famiglietti, J. S., Rodell, M., Chen, J. and Wilson, C. K. 2008. Analysis of terrestrial water storage changes from GRACE and GLDAS, Water Resour. Res., 44, W02433, doi: 10.1029/2006WR005779.

Tapley, B. D. , Bettadpur, S., Watkins, M. M. and Reigber, C. 2004a. The gravity recovery and climate experiment: Mission overview and early results. Geophys. Res. Lett., 31, L09607, doi: 10.1029 /2004GL019920.

Tapley, B. D., Bettadpur, S., Ries, J. C., Thompson, P. F. and Watkins, M. M. 2004b. GRACE measurements of mass variability in the Earth system, Science, 305: 503-505.

Velicogna, I. and Wahr, J. 2005. Greenland mass balance from GRACE, Geophys. Res. Lett., 32, L18505, doi: 10.1029/2005GL023955.

Vigo, I., Garcia, D. and Chao, B. F. 2005. Change in sea level trend in the Mediterranean and Black Seas. J. Mar. Res., 63 (6): 1085-1100.

Wahr, J., Swenson, S., Zlotnicki, V. and Velicogna, I. 2004. Time-variable gravity from GRACE: first results. Geophys. Res. Lett., 31, L11501, doi: 10.1029/2004GL019779.

Zlotnicki, V., Wahr, J., Fukumori, I. and Song, Y. T. 2007. Antarctic circumpolar current transport variability during 2003-05 from GRACE. J. Phys. Oceanog, 37 (2): 230-244.

Lagrangian Validation of the Mediterranean Mean Dynamic Topography by extraction of Tracer Frontal Structures

By Francesco d'Ovidio[1, 4], Vincent Taillandier[2], Isabelle Taupier-Letage[3], Laurent Mortier[4]

[1]Institut des Systèmes Complexes (ISC-PIF), Paris, France
[2]LOV-CNRS, Villefranche-sur-Mer, France
[3]Université de la Méditerranée-CNRS UMR 6535 Toulon, France
[4]LOCEAN-IPSL, 4 Place Jussieu; 75252 Paris, France

Abstract

In this work we test a new method for comparing a velocity field with the distribution of a tracer, in this case respectively altimetry-derived geostrophic currents and infrared SST images. We extract tracer fronts induced by altimetry velocities in the Eastern Mediterranean Sea with a Lagrangian technique: the Lyapunov exponent calculation. As a case study, we validate with this method the addition of the Mean Dynamic Topography (MDT) RioMed to sea surface height anomalies (SSA) in the Eastern Mediterranean Sea. At 100 km or more away from the coast, we find that fronts derived from absolute velocities match SST patterns better than fronts derived from velocity anomalies. However, close to the coast the MDT appears to strongly degrade the SSA signal by inducing a spurious folded pattern that is not present in SST images. This spurious pattern is probably due to an overestimation of the coastal currents. We suggest that this approach may be used for exploiting fine-scale structures of SST images in assimilation schemes.

Introduction

The near-surface circulation of the Mediterranean Sea is characterized by the presence of a rich variety of mesoscale structures (jets and eddies) which lifetime can range from few weeks up to several months and even years (Millot and Taupier-Letage, 2005). The interactions between jets and eddies play a key role on the distribution of material and thermohaline fluxes, acting either on the deflection of the coastal current offshore, or reciprocally on dispersing offshore water of the coastal zone (e.g. Hamad et al. 2005), thus advecting tracer anomalies at long range and influencing physical and biogeochemical properties (e.g. Taupier-Letage et al., 2003).

Altimetry data are a primary source of information on mesoscale transport and yield uninterrupted sea surface heights measurements (SSH) since 1993 (Pascual et al., 2006). Altimetry has documented the main properties of the mesoscale eddy activity and mixing in the Mediterranean Sea (Pujol and Larnicol, 2005, d'Ovidio et al., 2009). Velocity fields can be derived from SSH and estimated in gridded products (Ssalto/Duacs User Handbook, 2006). By exploiting the measurements of multiple altimetry satellites and by applying algorithms adapted to the complex topography of the Mediterranean basin, altimetry data allow to reconstruct surface velocities at a spatial resolution of 1/8 deg. and temporal resolution of 1 week.

Known limitations of altimetry-derived surface velocities are the errors associated with the altimetric measurement: these include less accurate measurements close to the coast where the altimetry signal is less reliable and the lack of velocity component above the geostrophic equilibrium approximation. A second limit of altimetry data comes from the indetermination in the shape of the geoid that hinders from an utilization of the absolute SSH measured from the satellites. In order to filter out heights due to the shape of the geoid and not to geostrophic balance, a 5-year mean is subtracted from the measurements, providing the Sea Surface Anomaly (SSA). This procedure removes not only the signal of the geoid, but also any current component with a non-zero mean over the 5-year period. In order to restore absolute velocities, a Mean Dynamic Topography (MDT), i.e., the stationary SSH corresponding to the 5-year mean, is added. The AVISO products use the RioMed MDT (Rio et al. 2007).

A possibility of validating altimetry-derived velocities and the MDT is offered by satellite observations of surface tracers like sea surface temperature (SST). In particular, infrared images are routinely used to infer information on the mesoscale circulation. These observations provide the temperature of the upper few microns of the sea (the so-called skin temperature). In some conditions, like in presence of a very shallow and temporary thermocline due to solar heating, SST images may present short-lived patterns (a few hours or less) that are not representative of the temperature of the mixed layer. However, images either obtained during nightly passes or following strong wind events, or with long-lived patterns (several days) are usually considered reliable signature of the mixed layer and of the surface circulation (Taupier-Letage 2008). Infrared SST images have a higher spatiotemporal resolution (up to 1km and better than 1 day) than altimetry gridded maps. However they require cloud-free conditions, and therefore are likely to provide patchy observations on both the spatial and temporal domains. Moreover, their quantitative interpretation in terms of transport is more complex than altimetry measurements, since their gradients depend on the effect of transport integrated over several days as well as on heat fluxes.

Therefore, several different approaches have been proposed for the validation of surface currents with SST images:

1) One of them consists in interpreting a mesoscale warm (resp. cold) anomaly as the signature of the depressed (doming) isopycnals associated with an anticyclonic (resp. cyclonic) eddy. However, due to wind surface mixing and jets/filaments entrained around eddies, the reverse case can also be found (Puillat et al. 2002, Hamad et al. 2006).

2) The Maximum Cross Correlation is another technique that uses consecutive images and provides a velocity field finding the local displacements that transform one image into the other (Bowen at al. 2002).

3) Recently, it has been also shown that a single SST snapshot contains under some conditions the information for reconstructing the full 3D velocity field up to 500m of depth (Isern-Fontanet et al. 2006, 2008).

In this work we propose a different technique aimed at comparing the expected spatial structure of a tracer advected by the mesoscale turbulence with the observed pattern of a real tracer like SST. The main difference in respect to other methods is that we reconstruct the *temporal* evolution of the tracer advection, obtaining in this way some spatial structures that are the results of both the spatial and the temporal variability of the velocity field. As a case study, we will apply this technique to the validation of the Mean Dynamic Topography in the Eastern Mediterranean Sea.

Data and method

The velocity fields we analyzed are the SSALTO/Duacs gridded, multimission absolute geostrophic velocities and geostrophic velocity anomalies (delayed time). For the period chosen (see table 1 below) two satellites where available: Jason-1 and Envisat. The Mediterranean Sea products are at a higher resolution (1/8 deg.) than the global ones (1/3 deg.) thanks to a specialized algorithm that takes into account the complex topography of the Mediterranean basin. The difference between the absolute velocities and the velocity anomalies is given by the RioMed MDT (Rio et al. 2007). The effect of the MDT on transport barriers and its possible signature in SST images are the aim of this work.

In order to validate the fronts deduced from the altimetry field, we used the brightness temperature images from the AVHRR channel 4 (~10.8 µm) that is less noisy than the signal obtained after a multichannel composition algorithm as a proxy of an advected tracer distribution. The use of relative values of temperature is not an important issue here, since we are only interested in the shape of the patterns. Thus we keep using the acronym SST.

We chose 11 images where SST structures were cloud-free in the region of our study (19°-25°E, 32°-36°N), (see table 1 below):

28/5/2006, 20:26

07/06/2006 11:57

17/06/2006, 11:55

18/06/2006, 09:18

23/06/2006, 20:29

24/06/2006, 00:52

27/06/2006, 20:37

28/06/2006, 11:43

06/07/2006, 12:01

22/07/2006, 01:07

26/07/2006, 11:58

Table 1

List of the dates of the SST images that were used.

These images are from nighttime passes, or it was checked that the spatial features analyzed lasted several days, in order to ensure that these patterns were representative of mixed layer dynamics.

Tracer fronts were extracted from altimetry data with the finite-size Lyapunov exponent technique (Ott, 1993; Boffetta et al., 2001; d'Ovidio et al., 2004; Waugh et al., 2006; d'Ovidio et al. 2009). The Lyapunov exponents are obtained at each position and time by calculating the separation of trajectories initialized nearby backward in time, recovering in this way the advection history that has shaped a tracer pattern. At point ***x*** and time ***t,*** calling $\boldsymbol{\delta_0}$ and $\boldsymbol{\delta}$ the inital and final trajectories' separation and $\boldsymbol{\Delta t}$ the time needed to reach the separation $\boldsymbol{\delta}$, the local Lyapunov exponent is defined as:

$$\lambda(x,t) = \frac{1}{\Delta t}\log\left(\frac{\delta}{\delta_0}\right).$$

The parameters and algorithm used closely follow d'Ovidio et al. (2004) with $\boldsymbol{\delta_0}$ =0.01 deg. and $\boldsymbol{\delta}$ =0.4 deg. Maxima of local Lyapunov exponents are typically organized in convoluted lines (sometimes referred as Lagrangian coherent structures, or manifolds of hyperbolic points), that have been shown to provide the location of tracer filament boundaries (Shadden et al., 2005, Lehahn et al. 2007). More precisely, we used a more advanced calculation that consists in finding the linear transformation ***M*** that evolves in time a parallelepiped centered in the point ***x***. By diagonalizing $\boldsymbol{M^tM}$ one can find the Lyapunov exponent and also the orientation of the front. More details on the use of the Lyapunov technique for front detection will be presented in the next section.

For the localization of coherent structures of the instantaneous velocity field (eddies) we used the Okubo-Weiss (OW) parameter. The OW parameter provides the dominance of the vorticity in respect to the strain rate. Calling ***u*** and ***v*** respectively the longitudinal and zonal component of the velocities, one can measure the normal and shear components of the strain $\boldsymbol{S_n}$ and $\boldsymbol{S_s}$ and the vorticity $\boldsymbol{\omega}$:

$$S_n = \frac{du}{dx} - \frac{dv}{dy}, S_s = \frac{du}{dy} + \frac{dv}{dx}, \omega = \frac{dv}{dx} - \frac{du}{dy}$$

Then the Okubo-Weiss parameter ***W*** is

$$W = s_n^2 + s_s^2 - \omega^2.$$

The OW parameter is positive in the regions where the strain prevails and negative in the regions dominated by the relative vorticity. A common criterion for the identification of the eddy interior is therefore $\boldsymbol{W<0.}$

Small-scale tracer fronts detected from a large-scale velocity field

We briefly review here the dynamical concepts that are at the basis of the analysis we perform. More details can be found in d'Ovidio et al. (2009) and Lehahn et al. (2007). The possibility of comparing the fine scale structure of high resolution tracer images (SST and chlorophyll) with altimetry data seems at first sight not possible, since tracer images have a resolution much higher than altimetry snapshots: these images typically contain filaments (widths of 10-50 km) that are the signature of the submesoscale dynamics, while altimetry data only provide mesoscale signal, at one order of magnitude larger scale.

Nevertheless, tracer distributions are not the instantaneous effect of the geostrophic velocities but depend on the temporal variability of the velocities, being the result of an advection process. Therefore, if the velocity field is not stationary, the distribution of an advected tracer does not match necessarily the spatial structure of the velocity field, but contains in its spatial structure also information on the temporal variability of the velocities. In particular, the interaction of spatial and temporal variability of the horizontal advection may induce a filamentation process that creates tracer gradients at scales smaller than the scale of the resolved eddies.

This concept is sketched in Figures 1-3, where a synthetic tracer is advected by altimetry-derived surface velocities. If the velocities were stationary during the advection process, the tracer would align its fronts with the streamlines, closely resembling the structure of the mesoscale turbulence (Figure 1). However, due to the temporal variability of the velocity field, the tracer fronts are not parallel to the streamlines and lobes and filaments appear. Looking at a tracer distribution like the one of Figure 2, one would be tempted to think that the filaments appearing there are due to a component of the velocity field unresolved by altimetry. Instead, the synthetic tracer has been advected solely with altimetry-derived velocity. In fact, part of the tracer submesoscale also depends on the the component of the velocity field unresolved by altimetry, but comparisons using real data (Lehahn et al. 2007, d'Ovidio et al. 2009) showed that observed tracer filaments can be well predicted by mesoscale-only advection. This can be also explained by the fact that the possibly unresolved submesoscale component is also affected by the mesoscale advection, depending on the distribution of active tracers like the density (Isern-Fontanet et al., 2008). Therefore,

unresolved small-scale may be expected to act on a tracer mostly in phase with the tracer pattern induced by the mesoscale turbulence.

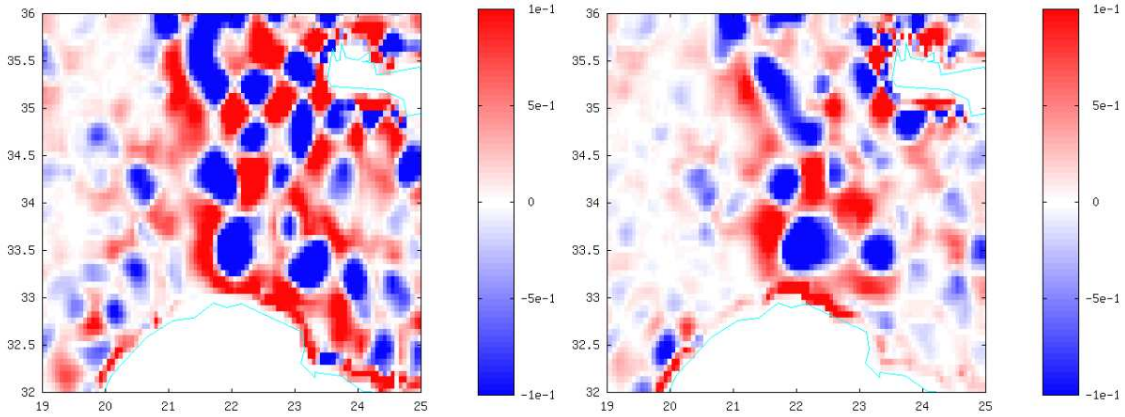

Figure 1

Okubo-Weiss parameter (1/s²) for the 26th of July 2006 from SSA (left) and SSH (right). Blue regions correspond to eddy cores. Note the strong effect of the MDT on the mesoscale dynamics.

The above discussion shows that in general it is correct to compare the streamlines of a flow with the pattern of a tracer only for very stationary velocity fields (e.g., topography constrained structures like the first Alboran gyre (see d'Ovidio et al. 2009). If on the contrary the velocity field evolves in time, its temporal variability will induce a signature on the *spatial* distribution of any advected tracer, typically in the form of filaments.

Coming back to the problem of the validation of a velocity field with an image of an advected tracer, one has therefore to answer the following question: how to combine in practice the information of the spatial and temporal variability of a velocity field for comparing with the spatial structure of the tracer?

There are several techniques that allow to solve this problem in a fairly straight way:

1) The simplest one can be the advection of a synthetic passive tracer like in Figure 2. This approach has however a limitation: the domain where the front appears (and up to some point, the shape of the front itself) is strongly dependent on the initial tracer distribution as well on the advection time.

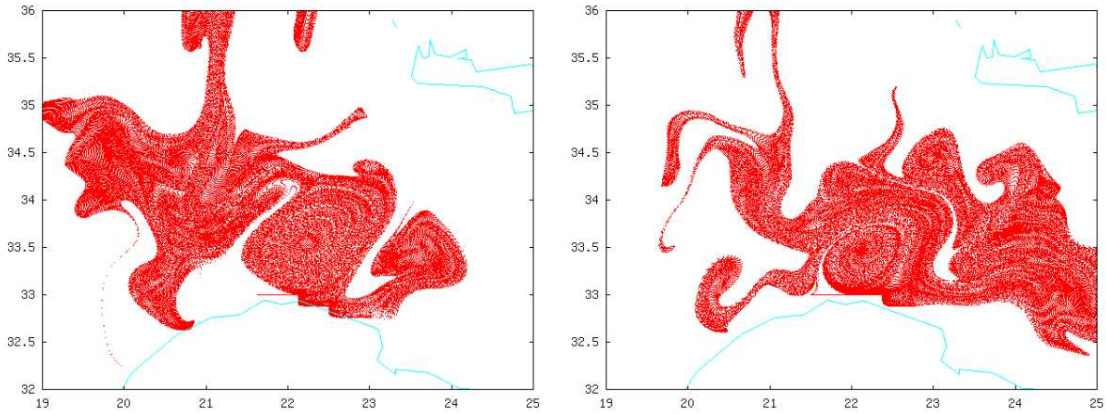

Figure 2

A tracer advected for two weeks until the 26th of July 2006 with velocities derived from the SSA (left) and SSH (right). The structure of the tracer distribution matches only qualitatively the eddy field (Fig. 1). This is pure Lagrangian effect due to the fact that the velocity field also evolves during the advection of the tracer.

2) A more precise technique consists in computing a map of finite-size (or finite-time) backward Lyapunov exponents. The backward Lyapunov exponent measures the rate of relative separation (on a prescribed spatial or temporal window) of the backward trajectories of particles in the neighborhood of a point. For finite-size exponents, the size of the neighborhood is a scale at which the velocity field is probed. In this work, this size is chosen at 1 km, in order to compare with the structure of SST images. With arguments of dynamical systems theory, it is possible to show that points with maxima of Lyapunov exponents are

organized in convoluted lines, and that these lines can be interpreted as the spatial structures over which tracer fronts are formed. The time scale of the front formation is related to the inverse of Lyapunov exponents, i.e., lines with larger Lyapunov exponents shape a tracer initialized nearby faster than regions with low Lyapunov exponents. In rough terms, and considering the definition of Lyapunov exponent as a measure of particle separation, the use of this tool for front detection is equivalent to the definition of a front as the line of fastest convergence for particles coming from regions far apart. Fronts obtained by computing maps of finite-size Lyapunov exponents from altimetry data have been compared with chlorophyll patches in the North East Atlantic (Lehahn et al. 2007) and SST filaments in the West Mediterranean Sea (d'Ovidio et al. 2009), with a remarkable agreement. Figure 3 shows an example of Lyapunov exponents for a day corresponding to one of the SST image and to the synthetic tracer of Figure 2. Lines of Lyapunov exponents of the order of 0.2 day^{-1} indicate that the mesoscale velocites align to these lines the gradient of a tracer released in this region in about 1/0.2=5 days.

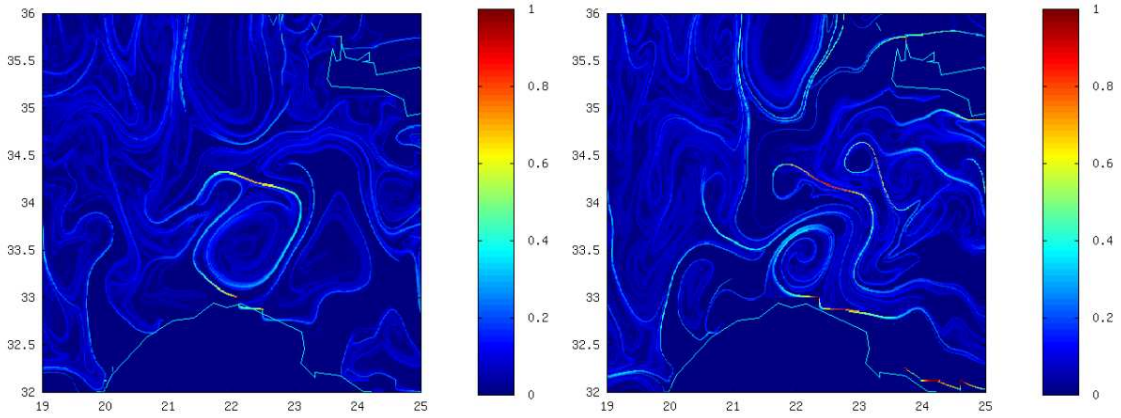

Figure 3

Map of Lyapunov exponents for the 26th of July 2006 derived from the SSA (left) and SSH (right). The Lyapunov exponent are obtained by integrating the velocities in time, and therefore can be directly compared with a tracer distribution (including submesoscale features). Maxima (ridges) of Lyapunov exponents correspond to the fronts of the tracer patches in Fig. 2.

Results

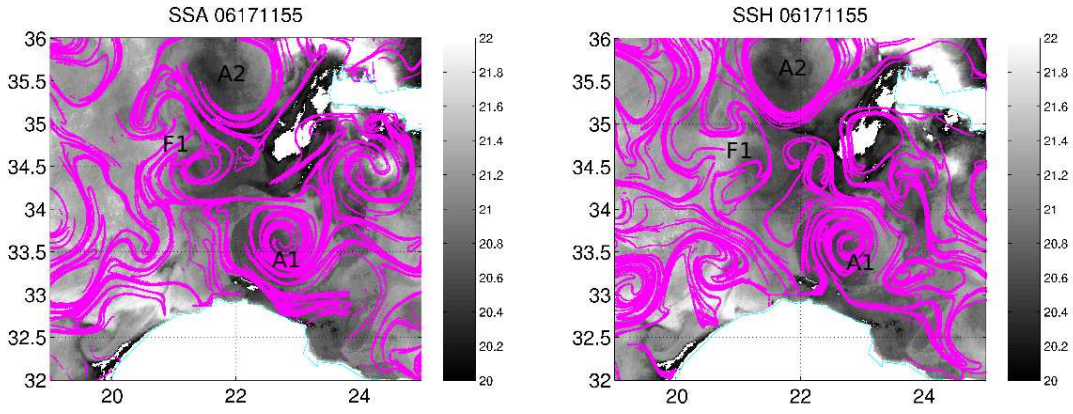

Figure 4

Superposition of SSA/SSH-derived fronts and SST patterns for the 17th of June 2006. The fronts are obtained by computing a map of Lyapunov exponents and keeping the values larger than 0.1 day^{-1} (see text for details).

The comparison between fronts extracted from SSA and SSH with the Lyapunov techniques and SST images is shown in Figures 4-6. On 17 June 2006 we see a mesoscale anticyclonic eddy (A1) along the Libyan coast with a colder core (due to wind mixing) and a plume of warmer water at its periphery (the drift of this eddy along the Libyan slope has been tracked during one year, see Taupier-Letage (2008)). A second anticyclonic eddy (A2) with weaker thermal gradient is also visible in 22°E, 35.5°N. Submesoscale filaments are present, althoug h blurred by high frequency noise. At 21°E, 34.5°N SST patterns suggest

a mushroom-like plume of warmer water approaching the anticyclone A2 from south-west (F1). Fronts reconstructed from both SSA and SSH correctly recognize A1 and A2. A1 is retrieved with a looser spiraling structure than A2, indicating a stronger water exchange with the environment. The position of A1 is better recovered from SSH (especially for the western flank). The front between A2 and Crete is almost perfectly identified in SSA fronts, but is quite distorted in the SSH ones. The mushroom-like feature F1 has a signature in both SSA and SSH filaments as an interacting eddy dipole, but its boundary with A1 seems to be better identified with SSA.

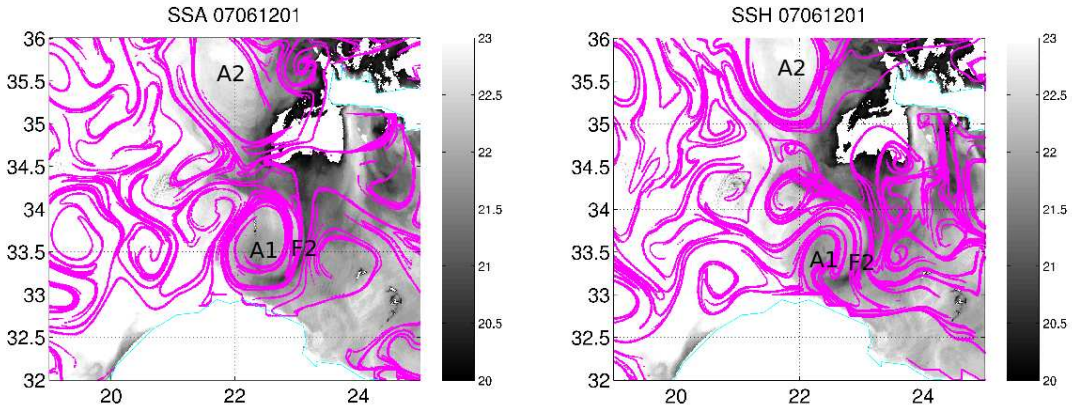

Figure 5

Same as Figure 4 for the 6th of July 2006.

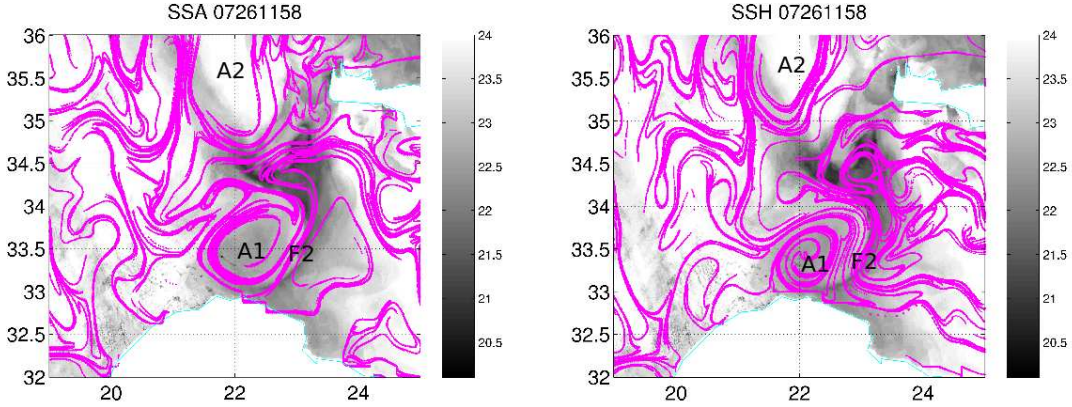

Figure 6

Same as figure 4 for the 26th of July 2006.

About one month after (6 July 2006) (figure 5) the SST signature of A1 shows a very small change while the thermal stratification in the environment of A2 does not allow delineating it sharply. The shape of A1 is well matched by both SSA and SSH fronts. However, SSA fronts almost perfectly reproduce a few kilometer-wide thin duct on the eastern flank of the eddy where a cold filament (F2) is entrained by the eddy. On the contrary, in the SSH case, the fronts are distorted when approaching the coast, intersecting the isotherms and indicating a spurious exchange of water from A1 with the coastal current.

The error of SSH fronts close to the Libyan coast is even more pronounced for the 26 July 2006. In this SST image we see again A1 close the Libyan coast, with the cold filament F2 winding further (clockwise) from north to south. This filament is very well detected by SSA-derived fronts, while fronts computed from SSH cross the filament isotherms almost perpendicularly as soon as the filament approaches the coast. SSH seems however to do a better job than SSA delimiting the anticyclone A2.

In order to improve the quantification of the comparisons between SSA/SSH-derived fronts and SST isotherms, we construct a map where we accumulate the match between fronts and isotherms orientation (Figure 7). The creation of this map requires heavy data processing, mainly due to the presence of noise and clouds that render the extraction of isotherm orientation quite challenging and very sparse. Specifically, we tried to reduce the effect of noise with an iterative Gaussian filter 3km wide (10 passes) and then we computed the gradient direction only in the region with relatively strong SST gradient (0.02 deg/km), interpolating in nearby points. The interpolation is necessary since Lyapunov manifolds do not match exactly the regions of strong gradients but may show displacements of a few km.

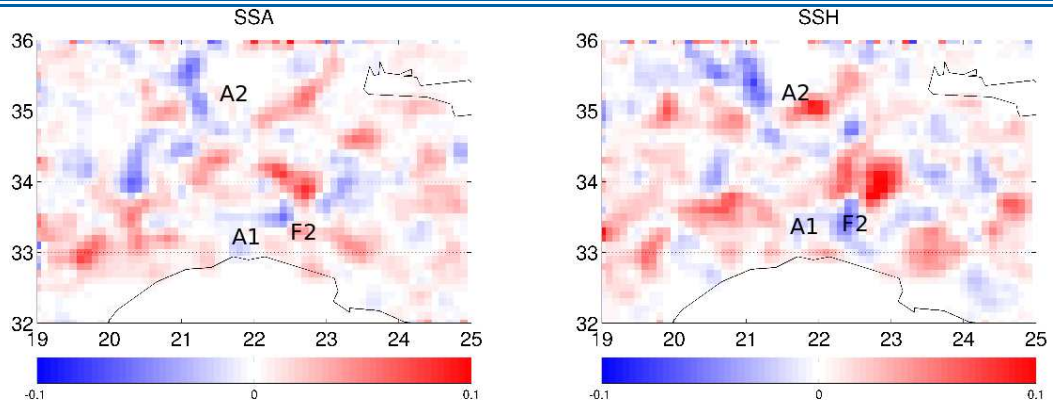

Figure 7

Average match of SSA/SSH-derived fronts with SST isotherms for the ensamble of 11 SST images. For each day and each pixel, we assign a score of one to the case in which a front intersects an isotherm with an angle less than 45 deg. (good match), a score of -1 corresponds to an intersection angle larger than 45 deg. and a score of zero if there are no fronts. The values showed in the figure indicate at each pixel the average of the score for the 11 days considered.

The orientation of the fronts is straightforward to calculate. It can be obtained by the Lyapunov algorithm itself, considering the stretching of a parallelepiped (see Ott, 1993 for the details) or it can be estimated by applying the gradient to the Lyapunov map. We compared the two approaches finding that they yield very similar results. We applied the gradient method for consistency with the SST analysis, restricting to the regions where the Lyapunov exponents are larger than 0.1 day^{-1}. These values correspond to a timescale for shaping a tracer front of about 10 days. After processing in this way SST and Lyapunov maps, we considered a score of 1 (good match) for the pixels where the isotherms and fronts intersect at an angle lower than 45 deg.. a score of -1 (mismatch) if the angle is larger than 45 deg. and zero otherwise. We computed this score for all the SST images selected and we averaged in space the result with a running squared window of 10km and then in time. Due to the paucity of the points where both requirements of clear sky, strong SST gradient and large Lyapunov exponent were verified at the same time, the map obtained in this way has a weak signal (with peaks around -0.1 and 0.1). The map shows that the MDT in many cases provides a positive contribution to the SSA for current estimations, peaking over the Aegean Plateau (23°E, 34°N). Nevertheless, there are regions where the SS A alone appears to work better, notably in the three sectors of the Libyan coast at 20°E, 22.5°E, and 24°E.

Discussion and conclusion

In this work we tested a new method for comparing a velocity field with the distribution of a tracer, in this case respectively altimetry-derived geostrophic currents and infrared SST images. As a case study, we have analyzed the effect of the Mean Dynamic Topography on the structure of tracer fronts along the Libyan coast. The method can be seen as a Lagrangian improvement of the traditional method. The basic idea behind is that the expected match between tracer isolines and streamlines is only valid at first approximation, when the temporal variability of the velocity field can be neglected. If the temporal variability of the velocity is also taken into account, a cascade from the meso- to the small-scales takes place, and the tracer fronts are not parallel to the velocities. In particular, some small-scale folds appear, that are the effect of transport integrated over time. The full structure of the expected tracer fronts can be reconstructed automatically from the velocity field with Lagrangian techniques like the Lyapunov exponent calculations. These lines, that look like perturbed altimetry streamlines, are thus the correct object that should be compared with the tracer contours.

We developed our analysis in two steps:

1) In the first one we have handpicked from the SST images some specific features (the boundary of an eddy, the intrusion of a filament,..) and looked at their corresponding front identified from SSA and SSH by the Lyapunov technique. When applied to a sequence of SST images, this approach is fairly solid, since one can check the temporal coherence of the match and mismatch.

2) Second, we attempted to generalize this comparison by computing the match between the direction of the fronts and that of the isotherms. This calculation yielded a map that helps to localize the regions where the MDT may be wrong, even if the sampling in space is very heterogenous and depends on the strongly non-uniform distribution of mesoscale eddies (and SST strong gradients). The comparison between fronts and isotherms has been done only where both SST gradients and Lyapunov exponents were high. This filter was intended to restrict the analysis to the most coherent structures, although it does not provide the confidence of a manual analysis.

The main result i) was the identification of some regions, mostly along the Libyan coast, where the MDT appears to actually degrade the SSA. This result is not completely surprising since the Eastern Mediterranean Sea is known to suffer of a lack of in situ observations, and therefore is a worst case scenario for the MDT; ii) A second interesting result is the observation that the MDT has a strong impact on the shape and intensity of the tracer fronts. Weak eddies, especially cyclonic ones, may be suppressed and even for very strong eddies like A1 the MDT induces important effects like the permeability of the eddy through a change in the shape of the filaments exchanged with the environment.

The main advantage of the approach described in this work is that the fronts reconstructed by Lagrangian methods contain some structure at a spatial scale smaller than the scale of the velocity field. Therefore, with this approach it is possible to exploit part of the high-resolution details of SST images for the validation of much coarser velocity fields like altimetry (see for instance the case of the filament F2). The main limitation on the other hand is the implicit assumption that the main driver behind the spatial structuration of the SST is the horizontal stirring. This hypothesis is basically the same behind other methods like the Maximum Cross Correlation technique. Note that the temperature value along the isotherm is not used, since only the isotherm shape is compared. In this regard, the hypothesis is more relaxed than the one behind other velocity reconstruction methods that exploit the active nature of the SST tracer, like the effective Surface Quasi-Geostrophy approach (Isern-Fontanet et al., 2008). The fact that only the tracer contour is needed (not the tracer absolute values) allows to apply this technique to other surface tracer, and notably high-resolution chlorophyll images. Another advantage is that the method can be applied to local features of SST or chlorophyll images, allowing the exploitation of images with strong cloud coverage. A possible improvement of this technique may come from using the singularity exponent calculation for extracting the isotherms in a more robust way (Turiel et al. 2005) and avoiding smoothing filters (that were instead required before applying the gradient).

One of the possible straightforward applications for this technique for an operational system such as MERCATOR is to provide a mapping of uncertainties that affect the MDT. Considering an extended set of SST or chlorophyll images and systematically computing the match between fronts such as the one given in Figure 6, the resulting map would contribute to quantify the observational error structure for the assimilation of altimetric products. Iteratively performed in parallel to other approaches (e.g. Dobricic, 2005), such diagnostic would significantly refine the spatial features of uncertainties on MDT allowing for instance to evaluate observational error covariances of the assimilation system. In perspective, the match between fronts and isotherms/chlorophyll isolines could also be used in a variational scheme that aims at finding the perturbation of the altimetry velocity field able to maximize the match.

Acknowledgments

The authors wish to thank the SATMOS (CNRS/INSU/MétéoFrance) for the thermal images. *The altimeter products were produced by Ssalto/*Duacs *and distributed by* Aviso *with support from* Cnes. VT was funded by the ANR project LIVINSTONE. FdO was partially supported by Cnes.

References

Boffetta, G., G. Lacorata, G. Redaelli, and A. Vulpiani (2001), Detecting barriers of transport: a review of different techniques. Physica D, 159, 58-70.

Bowen, M., J. Emery, P. Wilkin, P. Tildeshey, I. Barton, and R. Knewston (2002), Extracting multilayer surface currents from sequential thermal imagery using the maximum cross-covariance technique. J. Atmos. Oceanic Technol., 19, 1665-1676.

Dobricic, S. (2005), New mean dynamic topography of the Mediterranean calculated from assimilation system diagnostics, Geophys. Res. Lett., L11606.

d'Ovidio, F., V. Fernandez, E. Hernandez-Garcia, and C. Lopez (2004), Mixing structures in the Mediterranean Sea from finite-size Lyapunov exponents. Geophys. Res. Lett., 101029.

d'Ovidio, F., J. Isern-Fontanet, C. López, E. García-Ladona, E. Hernández-García (2009), Comparison between Eulerian diagnostics and the finite-size Lyapunov exponent computed from altimetry in the Algerian Basin", Deep Sea Res. I, 56, 15-31.

Hamad, N., C. Millot, and I. Taupier-Letage (2005), A new hypothesis about the surface circulation in the eastern basin of the Mediterranean sea. Prog. Oceanogr., 66, 287-298.

Isern-Fontanet, J., B. Chapron, G. Lapeyre, and P. Klein (2006), Potential use of microwave sea surface temperature for the estimation of ocean currents. Geophys. Res. Lett., L24608.

Isern-Fontanet, J., G. Lapeyre, P. Klein, and B. Chapron (2008), Three-dimensional reconstruction of oceanic mesoscale currents from surface information. J. of Geophys. Res., C09005.

Lehahn, Y., F. d'Ovidio and M. Lévy (2007) Stirring of the northeast Atlantic spring bloom: A

Lagrangian analysis based on multisatellite data, J. of Geophys. Res., C08005.

Millot, C, and I. Taupier-Letage (2005), Circulation in the Mediterranean Sea. In: Saliot A. (ed) The Mediterranean Sea, Handbook of Environmental Chemistry, vol 5, Part K. Springer-Verlag, Berlin Heidelberg, 29-66.

Ott, E. (1993), Chaos in dynamical systems, Cambridge Univ. Press.

Pascual, A., Y. Faugere, G. Larnicol, and P.-Y. Le Traon (2006), Improved description of the ocean mesoscale variability by combining four satellite altimeters. Geophys. Res. Lett., L02611.

Puillat I., Taupier-Letage, I., and Millot, C. (2002), Algerian eddies lifetime can near 3 years, J. of Mar. Sys. 31, 245-259.

Pujol, M.I., and G. Larnicol (2005), Mediterranean sea kinetic energy variability from 11 years of altimetric data. J. Mar. Sys., 58, 121-142.

Rio, M.-H., P.-M. Poulain, A. Pascual, E. Mauri, G. Larnicol, R. Santoleri (2007), A Mean Dynamic Topography of the Mediterranean Sea computed from altimetric data, in-situ measurements and a general circulation model. *J. Mar. Sys.* 65: 484-508 2007.

Shadden, S.C., F. Lekien, and J.E. Marsden (2005), Definition and properties of Lagrangian coherent structures from finite-time Lyapunov exponents in two-dimensional aperiodic flows. Physica D, 212, 271-304.

Ssalto/Duacs User handbook (2006), (M)SLA and (M)ADT near-real time and delayed time products,CLS-DOS-NT-06.034.

Taupier-Letage, I., I. Puillat, P. Raimbault, and C. Millot (2003), Biological response to mesoscale eddies in the Algerian Basin. J. Geophys. Res., 108, 3245-3267.

Taupier-Letage, I. (2008): On the use of thermal images for circulation studies: applications to the Eastern Mediterranean basin, in Remote sensing of the European seas, V. Barale and M. Gade Eds., Springer Netherlands, 153-164.

Turiel, A., Isern-Fontanet, J., Garcia-Ladona, E., and Font, J. (2005), Multifractal Method for the Instantaneous Evaluation of the Stream Function in Geophysical Flows, Phys. Rev. Lett. 95:104502.

Waugh, D.W., E.R. Abraham, and M. Bowen (2006), Spatial variations of stirring in the surface ocean: a case study of the Tasman sea. J. Phys. Oceanogr., 36, 526-542.

Operational Forecast of Glider trajectories during EGO 2008 operations in the Mediterranean Sea using Mercator Ocean Forecast

By Blandine L'Hévéder[1], Jean-Michel Lellouche[2], Pascale Lherminier[3], Laurent Mortier[4], Thierry Terre[5], Pierre Testor[6], Gaëtan Vinay[7]

[1] LOCEAN, 4 place Jussieu, 75252 Paris, France
[2] CERFACS, 42 avenue Gustave Coriolis, 31057 Toulouse cedex 01
[3] LPO, 29280 Plouzané, Brest, France
[4] ENSTA, Palaiseau, France
[5] LPO, 29280 Plouzané, Brest, France
[6] LOCEAN, 4 place Jussieu, 75252 Paris, France
[7] Mercator-Ocean, 8/10 rue Hermès, 31520 Ramonville st Agne, Toulouse, France

Abstract

In the framework of the European Gliding Observatories (EGO) initiative, coordinated operations took place in the North Western Mediterranean Sea during the winters 2007 and 2008. Fleets of about 10 gliders were deployed to observe the ocean interior, with scientific and also operational objectives. During these deployments, daily operational forecasts of the glider trajectories were carried out, using the Mercator-Ocean forecasts. After a description of the operational chain set up to compute the forecast trajectories, the dense network of glider observations will be used to validate locally the Mercator-Ocean forecast systems.

Introduction

The European Gliding Observatories (EGO) initiative is a network of several teams of oceanographers, interested in developing the use of gliders for ocean observations. A glider (Davis et al. 2003) is a new platform in oceanography, equivalent to a remotely steered profiling float. After several successful experiences carried out in varied oceanic environment, there is a consensus on its great potential. The partners of EGO have operated gliders for various purposes and at different sites (Atlantic, Mediterranean, South West and South East Pacific). Coordinated deployments have been set up to demonstrate the capability of a fleet of gliders to sample the ocean, with specific scientific and/or operational objectives. This new observational capacity for process studies and operational monitoring of the ocean physics and bio-geochemistry has been tested in the North Western Mediterranean Sea with gliders from IFM-GEOMAR (Germany), IMEDEA (Spain), LPO, LOCEAN, LOV (France) and NOCS (UK) in winter 2007 and 2008.

The North Western Mediterranean basin is perfectly suited for this kind of demonstration: the circulation is a basin scale cyclonic gyre populated by strong mesoscale and sub-mesoscale features (major uncertainty sources for physical numerical models), particularly during the winter when deep convection occurs. Indeed, those mesoscale features are generated by vertical mixing (with deep convection events in the central part) and/or by developing instabilities of larger scale currents. It is also the location of the largest Spring bloom in the Mediterranean Sea and so, presents a strong interest for biogeochemical studies (Lévy et al. 1999). Finally, the northern part of the gyre, the so-called Northern Current, flowing over the shelf break, significantly controls the circulation over the shallow part of the Gulf of Lions and shelf slope exchange of dissolved and particulate matter. If this current was better sampled, perspectives for societal applications concerning the marine environment and activities would arise.

A first EGO demonstration took place in winter 2007 where nine gliders were deployed in the North Western Mediterranean basin. This coordinated deployment of a glider fleet was a successful technological demonstration and the amount of data collected (3200 profiles delivered in real time to the Coriolis Data Center) demonstrate how intensively one can observe the ocean interior using such platforms in a particular area. During winter 2007, we observed that the very mild air temperature conditions triggered convection down to only 400m depth, which is not a proper deep convection event (Testor et al. 2007).

This successful demonstration and the motivation to observe a real convection event leads to a second EGO operation with the new deployment of nine gliders between January and April 2008, which will be described more precisely hereby (Testor et al. 2008).

A glider mission requires an important work for the deployment and recovery phase but also a permanent monitoring throughout the mission to pilot the glider. The remote steering of the gliders and real time data download are allowed by Iridium bidirectional link and carried out using “landstation” computers based in the partners institutions. Tools have been developed for the pilots to steer efficiently a glider, and moreover to manage a fleet of around ten gliders, including real time data processing and visualization to better control the glider missions (example for the glider hannon http://www.locean-ipsl.upmc.fr/gliders/GROUNDSTATION/HANNON). Forecasts of the trajectories of the fleet, based on the currents routinely

produced by Mercator, have also been carried out both to help the pilots reshaping the network regularly and to deliver the information about the glider positions to the Spanish and French marine security agencies. In return, the data collected by the real gliders were delivered in real time to the Coriolis Data Center, and in such a way could be assimilated in the Mercator-Ocean forecast simulations. All these routines (glider data visualization and forecast) were executed automatically and are part of an operational chain. In this paper, the glider forecasting part of the operational system will be described more particularly.

Forecasting glider trajectories

The ocean forecasts for the Mediterranean Sea were provided by two Mercator Atlantic operational systems: from June 2006 to August 2008, PSY2V2 (1/15e, grid of 5 to 7 km varying with the cosine of the latitude), and since September 2008, PSY2V3 (1/12e, grid of 3 to 9 km). Every week, the two-week forecasts performed by these two systems with daily outputs were downloaded. Every day and for each instrument, the "glider flight simulator OPAGLI " (L'Hévéder 2006) computed eight forecast trajectories along different directions, starting from the last known real surface position/time of the gliders, and ending up seven days later. A quasi-static flight model with parameterized ballast and attitude controls and full 3D-time oceanic currents (as well as temperature and density for ballast) provided by the Mercator circulation model is used to simulate the glider trajectory. The data collection by the glider in the fields of the OGCM is also simulated. For each glider of the fleet, the forecast trajectories were plotted with the ocean currents and salinity field of Mercator forecast for the current day. The figures were published on the web (example for the glider hannon on March 02 2008 http://www.locean-ipsl.upmc.fr/gliders/GLIDERFORECAST/HANNON).

The first operational forecast of a glider trajectory in summer 2006

This operational system has been tested for the first time in summer 2006 during a two-month deployment of a Spray glider in the Irminger Sea (http://gliderweb.ifm-geomar.de/mersea/gliders/spray004_position.html). The glider pilots have found this forecast tool very helpful: it provided with the oceanic environment around the glider position the possible glider deviations in all the directions. In that case, the main objective of the glider mission was to sample the East-Greenland current, which flows with a velocity of about 30 cm/s in the upper 500m (Bersch 1995). Steering a glider, which maximum velocity is about 40 cm/s, in order to cross such a current is not straightforward and the trajectory forecasts carried out with the Mercator forecast simulations have been very helpful to better choose the glider waypoints. The East-Greenland current was quite well represented in the Mercator simulations, although its direction did not follow exactly the real topographic contours (figure 1).

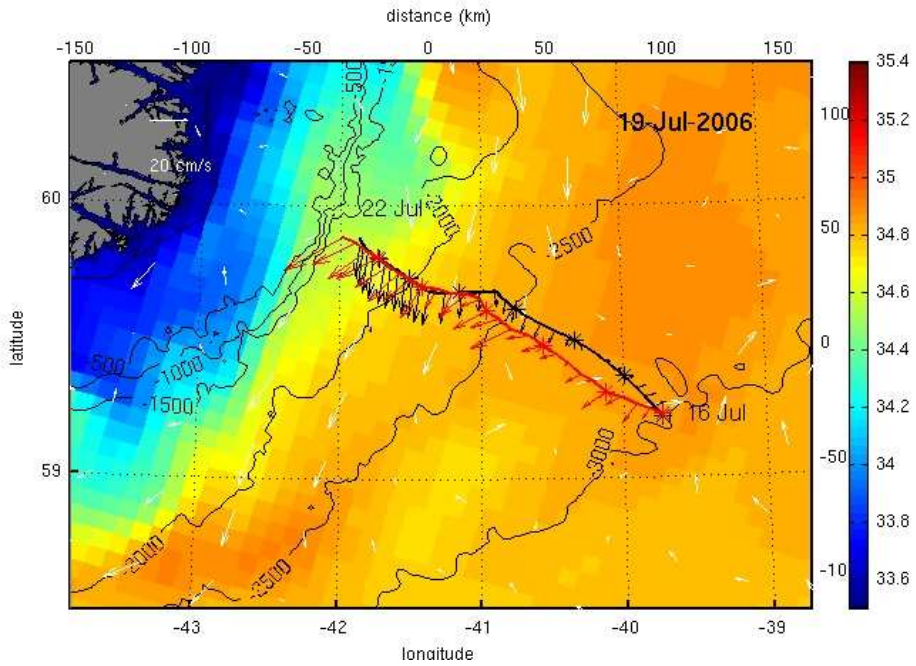

Figure 1

Surface currents (cm/s, scale in the top left part of the figure) and surface salinity (psu, right scale on the colorbar) field from Mercator forecast on 19-07-2006, superimposed with : 1) in red, the real glider spray004 trajectory between the 16th and the 22th July 2006 (red line and star every day) and the measured estimation of the 0-1000m averaged ocean velocity along this trajectory (red arrow); 2) in black, the daily glider forecast trajectory (black line and star) plotted with the forecast velocity averaged on 0-1000m (black arrow).

Operational forecast of a fleet of gliders trajectories during EGO 2007 and 2008 operations

During the first EGO operation in the North Western Mediterranean Sea in winter 2007, the system has been extended to a fleet of gliders, with different types of gliders (spray, slocum) and several “landstation” computers based in the EGO partners institutions (Paris, Villefranche S/mer, Spain, Italy, England, Germany,...). This system was completely operational for the second EGO operation conducted between January and April 2008. During this period, seven deep (1000m) and two shallow (200m) gliders were used to collect temperature and salinity profiles as well as oxygen, backscattering at several wavelengths, Chorophyll-a and CDOM fluorescence on the gliders equipped with biogeochemical sensors. One deep glider (named potame, see figure 2 for the position of the various gliders in March 2008) was devoted to the large scale monitoring of the gyre between the Balearic Islands and Banyuls. A shallow glider (named maya) was deployed to cross the channels between the Balearic Islands and a deep one (named hannon) sampled the Ligurian Sea offshore of Villefranche s/Mer to monitor an upstream section of the Northern Current. Three deep gliders (named ammonite, bellamite and coprolite) were devoted to the investigation of the deep convection area in the Gulf of Lion in the frame of the DOCONUG project. Finally, a shallow glider (named pytheas) and two deep gliders (named himilcon and ifm04) were deployed to sample the Northern Current flowing over the continental slope in the frame of the LIVINGSTONE project.

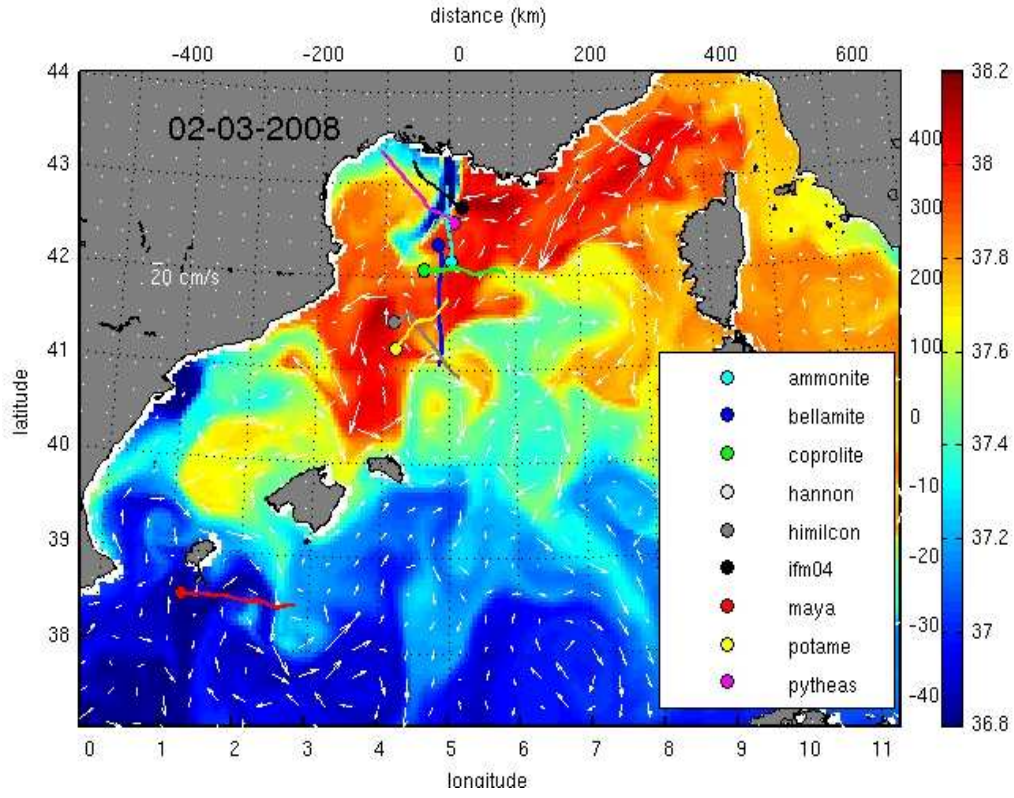

Figure 2

Surface currents (cm/s, scale in the top left part of the figure) and surface salinity (psu, right scale on the colorbar) field from Mercator forecast on 02-03-2008, superimposed with the gliders last positions (full color circles) and their 7-day forecast trajectories (color lines) towards the real waypoints aimed by the gliders.

A snapshot of the glider network on March 2nd 2008, with the nine glider positions as well as their forecast trajectories towards the waypoints aimed by each glider (figure 2) emphasize the complexity of the network and the utility of the forecast trajectories to help the pilots steering such a glider fleet.

At the surface on figure 2, the Mercator salinity field is quite realistic and the Northern Current can be highlighted along the continental slope (Millot 1999). The fresh water discharged by the Rhône can also be noticed. The forecast fields have a sufficient high resolution (about 6 km) to present various interesting mesoscale structures. In this rather realistic environment, the forecast trajectories of the nine gliders are not too much deviated by the oceanic currents. The gliders will be able to reach their waypoints more or less rapidly and directly. For example, one can note a small deviation to the North at the beginning of the trajectory of the glider himilcon (figure 2).

Moreover, the forecast system can be very useful in case of emergency glider recovery (empty batteries, technical problem ...). At the moment it is the only tool able to forecast the surfacing point using the ocean current forecasts.

Comparison between the glider data and Mercator forecast along a particular section

The section across the Ligurian Sea between Corsica and Villefranche S/mer has been sampled four times by the glider hannon and more particularly from South to North between the 14th and the 20th of February 2008. The real trajectory of the glider hannon during these seven days as well as its 7-day forecast trajectory, computed using the new Mercator system PSY2V3 have been plotted on figure 3. The simulated glider matches almost exactly the real glider trajectory, gliding in the same direction and at about the same velocity. Thanks to the relatively small ocean velocity along this section, the correction current option is very efficient and the glider follows an almost straight trajectory between two waypoints (represented by green stars on figure 3). Along this section, the ocean currents are located along the coast: the Western Corsica current flowing northeastward along the North Western coast of Corsica and the Northern Current flowing southwestward along the Villefranche S/Mer coast appear clearly on figure 3. The integrated ocean velocities measured by the simulated glider in the Mercator forecast fields are well located but underestimated. More particularly, the direction of the Northern Current is too westward oriented.

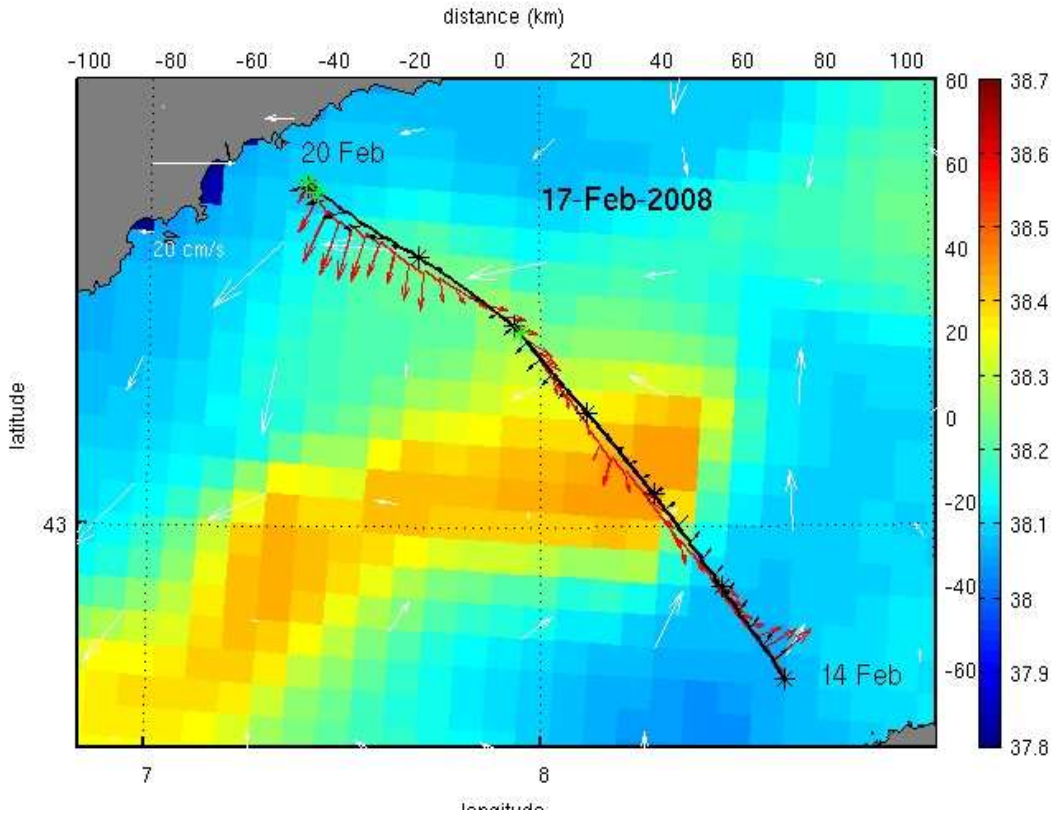

Figure 3

Surface currents (cm/s, scale in the top left part of the figure) and surface salinity (psu, right scale on the colorbar) field from Mercator forecast on Feb. 17 2008, superimposed with the glider hannon real and forecast trajectories between the 14th and the 20th February 2008 (respectively red and black line, stars and arrows) as on Figure 1.

The gliders provide very high resolution data (about 1 data per meter) along their trajectories. It is worth comparing the tracer fields sampled by the glider hannon along this section with what a simulated glider would have seen gliding along the same trajectory at the same time in the Mercator forecast fields (figure 4). On the temperature and salinity sections sampled by the glider hannon, the Levantine Intermediate Water can be recognized, flowing westward along the north coast, between 200m and 400m depth, and spread to the 2/3rd of the channel (Sparnocchia, 1995). At the surface and up to 100m depth, fresher water is advected by the coastal currents measured by the glider hannon (figure 4).

The temperature and salinity sections extracted from Mercator forecasts (PSY2V3 system) during these seven days are in quite good agreement with the data measured by the glider hannon. The Levantine Intermediate Water is present at the same depth, with similar characteristics (same salinity and a temperature slightly colder). Nevertheless, the water mass flowing northeastward along the Corsica is located too far offshore and the one flowing southwestward along the ligurian coast is not enough spread to the South. In the surface layer, the water temperature is underestimated of about 0.3 °C. Apart from these

small discrepancies, the water masses are quite realistic and the new Mercator system PSY2V3 give much better results in the Western Mediterranean Sea than what was observed in the former PSY2V2 system.

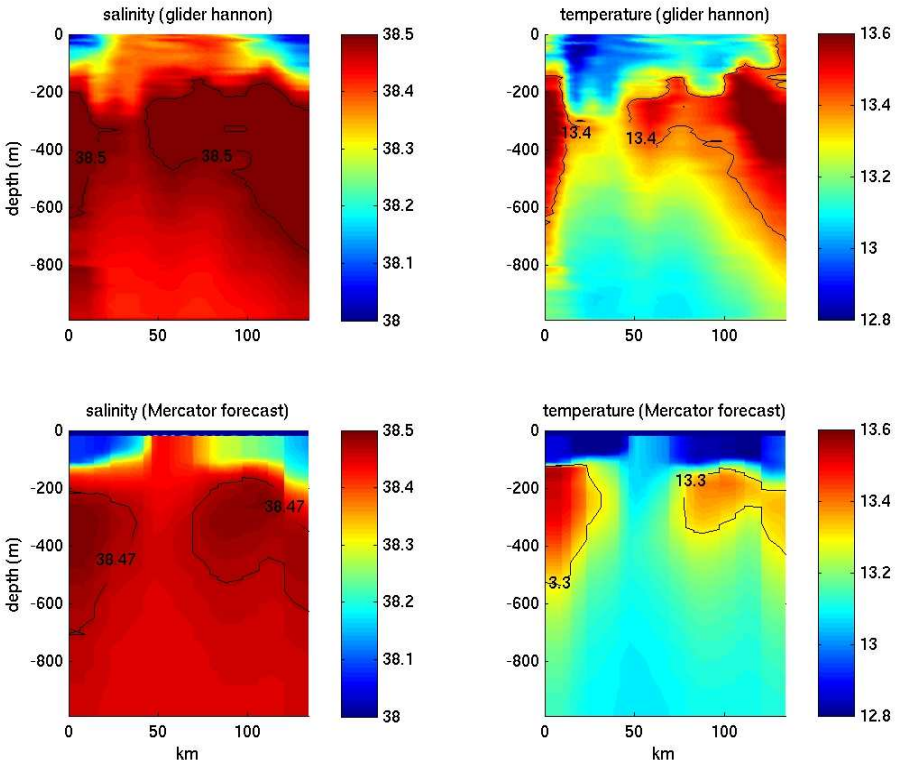

Figure 4

Salinity (psu) and temperature (°C) sections, i) on the top panels, measured by the glider hannon between the 14th and the 20th February 2008 and ii) on the lowers panels, forecasted by Mercator along the same section.

Conclusion

We have demonstrated that the Mercator forecasts can be of great help to steer a fleet of gliders in the North Western Mediterranean Sea, as well as in the Atlantic in summer 2006 for the spray glider. This approach can be systematically used for future glider operations in order to better dimension fixed transect of gliders as well as adaptative deployment to sample specific features. The relevance of the glider trajectory forecasts depends strongly on the realism of the numerical outputs. The dense network of observations that took place in winter 2007-2008 is now being used to benchmark it. In the PSY2V3 Mercator system, we have already shown that:

Along the coast, the average currents are well located but their steering angles present an error of about 30 to 40 degrees. In the Ligurian Sea, they are also underestimated, what is problematic for transport evaluation. On the other hand, the vertical distribution of water masses is well represented. In conclusion, thanks to altimetric data assimilation, the surface currents are realistic. Regarding the subsurface and deeper circulations, that need to be constrained in the longer term, shortcomings appear.

In order to continue improving the system, a GMMC PPR (Projet en Partenariat Renforcé) conducted jointly by Karine Béranger and the Mercator research team, beginning this year, will accordingly focus on the modeling and data assimilation methods in the Mediterranean Sea for the future operational Mercator systems.

In parallel, in the near future, it is planned that several gliders will operate together - all year round- in the Mediterranean Sea (MOOSE observatory in the North Western Mediterranean and more generally the “Chantier Méditerranée”) in order to feed the forecasting system. The operational chain we have presented will be used to pilot them.

References

Bersch, M. 1995: On the circulation of the northeastern North Atlantic. Deep-Sea Research, 42, 1583-1607.

Davis, R.E., C.E. Eriksen, C.P. Jones, 2003: Autonomous buoyancy-driven underwater gliders, in Technology and applications of autonomous underwater vehicles, G. Griffiths Ed., pp 37-58, Taylor and Francis. http://www-pord.ucsd.edu/~rdavis/publications/

Lévy, M., Mémery, L. and G. Madec, 1999: The onset of the spring bloom in the MEDOC area : mesoscale spatial varaibility, Deep-Sea Res., 46, 1137-1160.

L'Hévéder B., Mortier L. and Testor P., 2006: OPAGLI, a tool for the design and planning of glider observing networks , SeaTechWeek long abstract.

Millot C., 1999: Circulation in the Western Mediterranean Sea, J. Mar. Systems 20, 423-442.

Sparnocchia, S., Picco, P., Manzella, G., Ribotti, A., Copello, S. and P. Brosey, 1995 : Intermediate water formation in the Ligurian Sea, Oceanol. Acta 18 (2), 151-162.

P. Testor, L. Mortier, U. Send, R. Davis, D. Smeed, L. Merckelbach, G. Krahmann, J. Karstensen, H. Claustre, J.-J. Naudin, V. Rigaud, T. Carval, L. Petit de la Villeon, C. Jones and J. Sherman. : European Gliding Observatories (EGO), Coriolis Newsletter, October 2007

P. Testor, L. Mortier, B. Lheveder, V. Taillandier, U. Send, D. Smeed, L. Merckelbach, A. Alvarez, J. Tintore, B. Casas, S. Ruiz, P. Lherminier, T. Terre, G. Krahmann, J. Karstensen, F.Bourrin, H. Claustre, J.-J. Naudin, V. Rigaud, T. Carval, L. Petit de la Villeon, C. Jones, J. Sherman : Regional in-situ observatory : glider observations in the northwestern Mediterranean Sea in winter 2008, SCOR meeting.

Notebook

Editorial Board:

Laurence Crosnier

Secretary:

Monique Gasc

Articles:

The Hymex program: The specific context of oceanography

By Philippe Drobinski et al

Towards high resolution coastal and shelf circulation modeling

By Clothilde Langlais, Bernard Barnier and Philippe Fraunie

Ocean circulation in the Mediterranean Sea

By Jean-Paul Boy, David Garcia, Scott B. Luthcke, David D. Rowlands and Douglas S. Chinn

Lagrangian validation of the Mediterranean mean dynamic topography by extraction of tracer frontal structures

By Francesco d'Ovidio, Vincent Taillandier, Isabelle Taupier-Letage and Laurent Mortier

Operational forecast of glider trajectories during EGO 2008 operations in the Mediterranean Sea using Mercator-Ocean forecast

By Blandine l'Hévéder, Jean-Michel Lellouche, Pascale Lherminier, Laurent Mortier, Thierry Terre, Pierre Testor and Gaëtan Vinay

Contact :

Please send us your comments to the following e-mail address: webmaster@mercator-ocean.fr

Next issue: April 2009